Inorganic Chemistry

pubs.acs.org/IC Article

# Systematic Investigation of the Molecular and Electronic Structure of Thorium and Uranium Phosphorus and Arsenic Complexes

Michael L. Tarlton, O. Jonathan Fajen, Steven P. Kelley, Andrew Kerridge,* Thomas Malcomson, Thomas L. Morrison, Matthew P. Shores,* Xhensila Xhani, and Justin R. Walensky*

Cite This: *Inorg. Chem.* 2021, 60, 10614–10630 Read Online

ACCESS | Metrics & More | Article Recommendations | Supporting Information

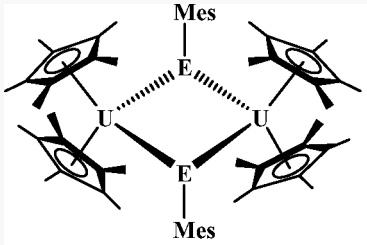


Mes = 2,4,6-$Me_3C_6H_2$

| | E = P | E = As |
|---|---|---|
| $\mu_{eff}$ (300 K) | 2.60 | 3.30 |
| $E_{1/2}$ U(IV/III) | -2.358 V | -2.316 V |
| DI (QTAIM) | 0.731 | 0.734 |
| U-E distance | 2.742(3) Å | 2.8310(4) Å |

**ABSTRACT:** In continuing to examine the interaction of actinide-ligand bonds with soft donor ligands, a comparative investigation with phosphorus and arsenic was conducted. A reaction of $(C_5Me_5)_2AnMe_2$, An = Th, U, with 2 equiv of $H_2AsMes$, Mes = 2,4,6-$Me_3C_6H_2$, forms the primary bis(arsenido) complexes, $(C_5Me_5)_2An[As(H)Mes]_2$. Both exhibit thermal instability at room temperature, leading to the elimination of $H_2$, and the formation of the diarsenido species, $(C_5Me_5)_2An(\eta^2\text{-}As_2Mes_2)$. The analogous diphosphido complexes, $(C_5Me_5)_2An(\eta^2\text{-}P_2Mes_2)$, could not be synthesized via the same route, even upon heating the bis(phosphido) species to 100 °C in toluene. However, they were accessible via the reaction of dimesityldiphosphane, MesP(H)P(H)Mes, with $(C_5Me_5)_2AnMe_2$ at 70 °C in toluene. When $(C_5Me_5)_2AnMe_2$ is reacted with 1 equiv of $H_2AsMes$, the bridging $\mu_2$-arsinidiide complexes $[(C_5Me_5)_2An]_2(\mu_2\text{-}AsMes)_2$ are formed. Upon reaction of $(C_5Me_5)_2UMe_2$ with 1 equiv of $H_2PMes$, the phosphinidiide $[(C_5Me_5)_2U(\mu_2\text{-}PMes)]_2$ is isolated. However, the analogous thorium reaction leads to a phosphido and C−H bond activation of the methyl on the mesityl group, forming $\{(C_5Me_5)_2Th[P(H)(2,4\text{-}Me_2C_6H_2\text{-}6\text{-}CH_2)]\}_2$. The reactivity of $[(C_5Me_5)_2An(\mu_2\text{-}EMes)]_2$ was investigated with $OPPh_3$ in an effort to produce terminal phosphinidene or arsinidene complexes. For E = As, An = U, a U(III) cation−anion pair $[(C_5Me_5)_2U(\eta^2\text{-}As_2Mes_2)][(C_5Me_5)_2U(OPPh_3)_2]$ is isolated. The reaction of $[(C_5Me_5)_2Th(\mu_2\text{-}AsMes)]_2$ with $OPPh_3$ does not result in a terminal arsinidene but, instead, eliminates $PPh_3$ to yield a bridging arsinidiide/oxo complex, $[(C_5Me_5)_2Th]_2(\mu_2\text{-}AsMes)(\mu_2\text{-}O)$. Finally, the combination of $[(C_5Me_5)_2U(\mu_2\text{-}PMes)]_2$ and $OPPh_3$ yields a terminal phosphinidene, $(C_5Me_5)_2U(=PMes)(OPPh_3)$, featuring a short U−P bond distance of 2.502(2) Å. Electrochemical measurements on the uranium pnictinidiide complexes demonstrate only a 0.04 V difference with phosphorus as a slightly better donor. Magnetic measurements on the uranium complexes show more excited-state mixing and therefore higher magnetic moments with the arsenic-containing compounds but no deviation from uncoupled U(IV) behavior. Finally, a quantum theory of atoms in molecules analysis shows highly polarized actinide-pnictogen bonds with similar bonding characteristics, supporting the electrochemical and magnetic measurements of similar bonding between actinide-phosphorus and actinide-arsenic bonds.

## INTRODUCTION

The structural characteristics and fundamental chemical behavior of actinide complexes bearing soft donor ligands have become increasingly relevant to the design of radionuclide remediation processes, as these ligands serve a role as extractants.[1−7] Such ligands are employed to more efficiently separate actinides from the chemically similar lanthanides, owing to the actinides' greater selectivity for soft donors over the more common N and O donors with the greater covalent character of actinide soft-donor bonds suggested as the reason for this selectivity.[8−10] However, the paucity of studies comparing structure, bonding, and reactivity properties of actinide complexes containing heavier main group elements[11−22] hinders the development of potential separation applications. This is especially true of arsenic, which is poorly represented in the organoactinide literature.[21,23−31]

Received: April 24, 2021
Published: June 30, 2021

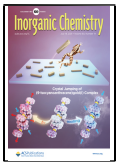







https://doi.org/10.1021/acs.inorgchem.1c01256
*Inorg. Chem.* 2021, 60, 10614−10630

One of the emerging developments in elucidating this phenomenon is the energy-driven-covalency concept in which the energy difference between the 5f orbitals and the *n*p orbitals decreases with increasing *n*.[32−34] While it has been shown that this does not lead to stronger covalent bonds,[35] to probe this concept in more depth, our laboratory, along with others, has been examining the structure, bonding, and reactivity of actinide-pnictogen bonds. Investigating this concept will afford insight into the fundamental coordination chemistry of these understudied metals as well as the potential to lead to advanced strategies in separation technologies. There are a number of phosphido complexes of thorium and uranium[36] but few examples of arsenido,[21,23−28,30,31] diphosphido,[37−39] diarsenido,[24,31] phosphinidiide,[26,40−42] arsinidiide,[24,26] phosphinidene,[37,43−48] and arsinidene,[23,49,50] Scheme 1. Recently, a diuranium complex containing a $(P_2)^{2-}$ unit was reported.[51] However, few analogous phosphorus and arsenic complexes have been synthesized to make valid comparisons; thus, we have sought to bridge this knowledge gap.

**Scheme 1. Functional Groups of Phosphorus and Arsenic Involved in This Work**

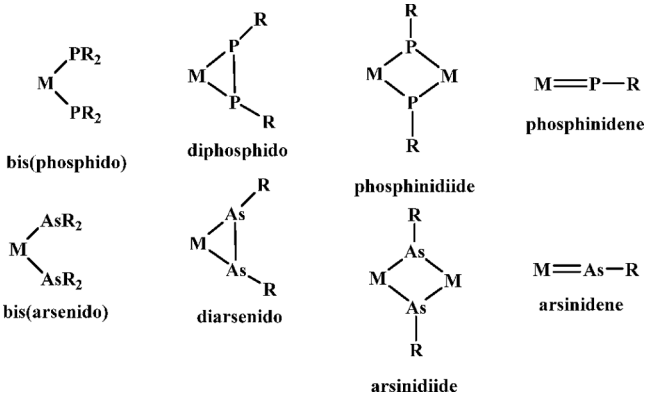


Herein, we describe the synthesis and characterization of a series of new actinide complexes with metal−phosphorus and metal−arsenic bonds, their molecular and electronic structures, and reactivity with $OPPh_3$ to achieve actinide-ligand multiple-bonding. Magnetic and electrochemical measurements on the uranium complexes were also undertaken to probe differences in bonding, and all complexes were studied using quantum theory of atoms in molecules (QTAIM) analysis (density functional theory (DFT)) to examine the energy-driven covalency concept.

## EXPERIMENTAL SECTION

**General Considerations.** All reactions were performed under an inert atmosphere of dry $N_2$ inside a glovebox. $MesAsH_2$,[52] MesP(H)-P(H)Mes,[53] $(C_5Me_5)_2AnMe_2$ (An = Th, U),[54] and $(C_5Me_5)_2ThMe(I)$[55] were prepared according to literature procedures. Solvents were dried via activated alumina and dispensed through a solvent-purification system, MBRAUN. $C_6D_6$ (Cambridge Isotope Laboratories) was subjected to three freeze−pump−thaw cycles and dried over activated 4 Å molecular sieves for 72 h prior to use. All $^1H$ and $^{13}C\{^1H\}$ NMR experiments were performed on a 500 or 600 MHz Bruker NMR spectrometer. Spectra were referenced to residual $C_6D_5H$ at 7.16 ppm ($^1H$) and 128.06 ppm ($^{13}C\{^1H\}$), respectively. All $^{31}P$ NMR experiments were done on a 300 MHz Bruker NMR spectrometer, and chemical shifts were referenced externally to $H_3PO_4$ at 0 ppm. IR spectra were collected from samples prepared as KBr plates with a Nicolet Summit PRO FTIR spectrometer. Elemental analyses were performed by the Microanalytical Facility, University of California, Berkeley.

***Caution!*** *Thorium-232 and depleted uranium (primarily U-238) are α-emitting radiometals with half-lives of* $1.4 \times 10^{10}$ *years and* $4.47 \times 10^9$ *years, respectively. All work was performed in a radiological laboratory with appropriate personal protective and counting equipment.*

*Synthesis of* $(C_5Me_5)_2Th[As(H)Mes]_2$, **1**. A colorless, 5 mL pentane solution of $H_2AsMes$ (757 mg, 3.86 mmol) was added dropwise to a stirring, 5 mL, pentane slurry of $(C_5Me_5)_2ThMe_2$ (822 mg, 1.54 mmol) at −30 °C. The mixture was allowed to warm to ambient temperature and stirred for 2 h, during which time the color of the reaction mixture progressed from colorless to yellow, to yellow/orange, then to deep orange with precipitation of a large amount of a fine orange solid. The mixture was then filtered over an M-porosity fritted glass funnel and washed with 4 mL of cold (−30 °C) pentane two times, leaving a bright orange solid on the filter. The volatiles were removed under vacuum, leaving **1** as an analytically pure, bright orange powder, 1.09 g, 79%. Crystals of **1** suitable for X-ray crystallography were grown from a concentrated diethyl ether solution at −30 °C. $^1H$ NMR ($C_6D_6$, 600 MHz, 25 °C): $\delta$ 6.98 (s, 4H, *m*-H), 2.63 (s, 12 H, *o*-$CH_3$), 2.51 (s, 2H, As−H), 2.34 (s, 6H, *p*-$CH_3$), 1.92 (s, 30H, $C_5Me_5$). $^{13}C\{^1H\}$ NMR ($C_6D_6$, 150 MHz): $\delta$ 143.1 (s, *p*-$C_{aryl}$), 140.0 (s, *o*-$C_{aryl}$), 134.24 (s, *i*-$C_{aryl}$), 127.5 (s, $C_5Me_5$), 26.68 (s, *o*-$CH_3$), 20.93 (s, *p*-$CH_3$), 11.73 (s, $C_5Me_5$), resonance for *m*-C(H) overlaps with signal from residual $C_6D_5H$. IR ($cm^{-1}$): 2953 (s), 2900 (s), 2855 (s), 2725 (w), 2090 (m), 1712 (w), 1600 (w), 1550 (w), 1456 (s), 1375 (m), 1261 (m), 1091 (m), 1022 (s), 845 (s), 802 (m), 705 (w), 684 (w), 611 (w), 543 (w). Elemental analysis calculated for $C_{38}H_{54}As_2Th$ (892.71 g/mol): C, 51.13%; H, 6.10%. Found: C, 50.77%; 5.84%.

*Synthesis of* $(C_5Me_5)_2U[As(H)Mes]_2$, **2**. A 6 mL, deep orange, $Et_2O$ solution of $(C_5Me_5)_2UMe_2$ (252 mg, 0.468 mmol) was added dropwise to a stirring, colorless, 5 mL $Et_2O$ solution of $H_2As$-Mes (200 mg, 1.02 mmol) at room temperature. The color became darker within 5 min, and the mixture was left to stir for 2.5 h. After filtration through diatomaceous earth, the mixture was concentrated to a black solid, then dissolved in 2 mL of pentane and cooled to −30 °C in a glovebox freezer to facilitate crystallization. The solution grew a crop of black crystals that were collected by filtration over a medium-porosity glass frit and washed with another portion of room-temperature pentane (8 mL). A black, microcrystalline powder remained, 335 mg, 80%. Crystals of **2** suitable for X-ray crystallography were grown from a concentrated pentane solution at −30 °C. $^1H$ NMR (600 MHz, $C_6D_6$, 25 °C): $\delta$ 15.43 (s, 30H, $C_5Me_5$), 5.04 (s, 6H, *p*-$CH_3$), 2.95 (s, 4H, *m*-H), −24.3 (s, 12H, *o*-$CH_3$), −151.1 (s, br, 2H, As-H). IR ($cm^{-1}$): 2935 (m), 2896 (s), 2853 (m), 2723 (s), 2093 (m), 1599 (w), 1549 (w), 1456 (s), 1375 (s), 1261 (w), 1173 (w), 1046 (w), 1021(s), 845 (s), 804 (w), 704 (w), 602 (w), 543 (w). The thermal instability of **2** at room temperature made elemental analysis not possible.

*Synthesis of* $(C_5Me_5)_2Th(\eta^2\text{-}As_2Mes_2)$, **3**. A 5 mL, colorless toluene solution of $H_2AsMes$ (225 mg, 1.2 mmol) was added dropwise to a stirring, white slurry of $(C_5Me_5)_2ThMe_2$ (300 mg, 0.563 mmol) in 5 mL of toluene. The mixture was heated to 75 °C overnight, causing a color change from yellow to orange-red over the first 2 h and, finally, to a dark green after being stirred for 12 h. The solution was filtered through diatomaceous earth, and then the volatiles were removed under vacuum, triturated in pentane, then collected over an F-porosity fritted glass funnel, leaving a green powder, 351 mg, 70%. Crystals suitable for X-ray diffraction were grown from an $Et_2O$ solution at −30 °C. $^1H$ NMR ($C_6D_6$, 600 MHz, 25 °C): $\delta$ 6.94 (s, 4H, *m*-H), 2.57 (s, 12H, *o*-$CH_3$), 2.35 (s, 6H, *p*-$CH_3$), 1.92 (s, 30H, $C_5Me_5$). $^{13}C\{^1H\}$ NMR ($C_6D_6$, 150 MHz): $\delta$ 144.06 (s, *o*-$C_{aryl}$), 133.04 (s, *p*-$C_{aryl}$), 128.16 (s, *m*-$C_{aryl}$), 127.98 (s, *i*-$C_{aryl}$), 126.59 (s, $C_5Me_5$), 26.86 (s, *o*-$CH_3$), 20.51 (s, *p*-$CH_3$), 10.94 (s, $C_5Me_5$). IR ($cm^{-1}$): 2959 (s), 2919 (s), 2853 (s), 2724 (w), 2107 (w), 1644 (w), 1598 (w), 1451 (m), 1376 (m), 1261 (m), 1095 (s), 1044 (s), 1022 (s), 848 (w), 803 (m). Elemental analysis calculated for $C_{38}H_{52}As_2Th$ (890.70 g/mol): C, 51.24%; H, 5.88%. Found: C, 50.91%; 5.74%.

*Synthesis of* $(C_5Me_5)_2U(\eta^2\text{-}As_2Mes_2)$, **4**. A 100 mL Strauss flask was charged with $(C_5Me_5)_2UMe_2$ (143 mg, 0.266 mmol) and 20 mL of toluene. To this stirring red solution was added $H_2AsMes$ (111 mg,


https://doi.org/10.1021/acs.inorgchem.1c01256
Inorg. Chem. 2021, 60, 10614−10630

0.566 mmol). The resulting dark red-black solution was then heated at 80 °C overnight. The solution was allowed to cool to room temperature, and the volatiles were removed under vacuum, leaving a black solid, which was triturated with ∼3 mL of pentane and dried again, leaving a black powder, 122 mg, 51%. Crystals of **4** suitable for X-ray diffraction were grown from a concentrated $Et_2O$ solution at −30 °C. $^1$H NMR ($C_6D_6$, 600 MHz, 25 °C): $\delta$ 7.57 (s, 30H, $C_5Me_5$), 1.41 (s, 6H, *p*-$CH_3$). The *o*-$CH_3$ and aryl-H resonances in **4** were not observable at room temperature or with variable-temperature NMR spectroscopy. IR ($cm^{-1}$): 2961 (s), 2910 (s), 2855 (s), 2723 (w), 2105 (w), 1627 (w), 1599 (w), 1558 (w), 1450 (s), 1375 (m), 1269 (w), 1261 (m), 1082 (m), 1021 (s), 846 (m), 800 (m). Elemental analysis calculated for $C_{38}H_{52}As_2U$ (896.69 g/mol): C, 50.90%; H, 5.84%. Found: C, 50.67%; 5.92%.

*Synthesis of* $(C_5Me_5)_2Th(\eta^2\text{-}P_2Mes_2)$, **5**. In a glovebox, a 5 mL toluene solution of MesP(H)P(H)Mes (247 mg, 0.817 mmol) was added to a 50 mL Strauss flask containing a 15 mL toluene solution of $(C_5Me_5)_2ThMe_2$ (435 mg, 0.817 mmol), sealed, brought out of a glovebox, and heated with stirring to 70 °C for 24 h. The color became dark green, then brown, over the course of the reaction. The flask was brought back into a glovebox, the volatiles were removed under vacuum, and the residue was extracted in 3 mL of $Et_2O$ twice, filtered through diatomaceous earth, and concentrated to ∼2 mL. Cooling to −40 °C in a glovebox freezer facilitated the growth of dark green crystals over ∼16 h, which were isolated, rinsed with 2 mL of cold pentane twice, and stripped of volatiles under vacuum, 430 mg, 67%. $^1$H NMR (600 MHz, $C_6D_6$, 25 °C): $\delta$ 6.89 (s, 4H, *m*-H), 2.64 (s, 12H, *o*-$CH_3$), 2.32 (s, 6H, *p*-$CH_3$), 1.90 (s, 30H, $C_5Me_5$). $^{13}$C{$^1$H} NMR ($C_6D_6$, 150 MHz): $\delta$ 143.56 (t, $^1J_{C-P}$ = 114 Hz), 140.98 (s, *o*-$C_{aryl}$), 132.36 (s, *p*-$C_{aryl}$), 129.22 (s, *m*-$C_{aryl}$), 126.77 (s, $C_5Me_5$), 126.12 (t, $^3J_{C-P}$ = 36 Hz, *o*-$CH_3$), 20.83 (s, *p*-$CH_3$), 11.37 (s, $C_5Me_5$). $^{31}$P{$^1$H} NMR ($C_6D_6$, 101 MHz, 25 °C): $\delta$ 58.92 (s). IR ($cm^{-1}$): 2956 (s), 2897 (s), 2856 (s), 2725 (w), 1601 (w), 1453 (s), 1376 (s), 1262 (m), 1173 (w), 1096 (m), 1042 (s), 1022 (s), 949 (w), 849 (m), 712 (w), 616 (w), 547 (w). Elemental analysis calculated for $C_{38}H_{52}P_2Th$ (802.80 g/mol): C, 56.85%; H, 6.53%. Found: C, 57.00%; 6.36%.

*Synthesis of* $(C_5Me_5)_2U(\eta^2\text{-}P_2Mes_2)$, **6**. In a glovebox, a 10 mL toluene solution of $(C_5Me_5)_2UMe_2$ (267 mg, 0.496 mmol) was added to a 50 mL round-bottom Strauss flask followed by a 5 mL toluene solution of MesP(H)P(H)Mes (150 mg, 0.496 mmol). The flask was sealed and heated to 70 °C with stirring. The mixture darkened to a dark brown/black within 5 min, and then after 1 h of total stirring, the volatiles were removed under vacuum, leaving a black/brown solid. The flask was brought back into a glovebox, and the crude product was extracted in 15 mL of $Et_2O$ twice, filtered through diatomaceous earth, and concentrated to a black solid. The solid was triturated in 5 mL of pentane and collected over an M-porosity glass frit, followed by a wash with 5 mL more of pentane, leaving a microcrystalline, black solid, which was collected, and the volatiles were removed under vacuum again, 195 mg, 49%. $^1$H NMR (600 MHz, $C_6D_6$, 25 °C): $\delta$ 5.05 (s, 30H, $C_5Me_5$), 3.73 (s, 6H, *p*-$CH_3$), 1.23 (s, 4H, *m*-H), −22.26 (s, br, 12H, *o*-$CH_3$). IR ($cm^{-1}$): 2960 (s), 2907 (s), 2856 (s), 2723 (w), 2329 (w), 1719 (w), 1632 (w), 1602 (m), 1452 (s), 1376 (s), 1290 (w), 1261 (m), 1095 (s), 1022 (s), 849 (m), 804 (m), 712 (w), 603 (w), 548 (w), 497 (w). Elemental analysis calculated for $C_{38}H_{52}P_2U$ (808.79 g/mol): C, 56.43%; H, 6.48%. Found: C, 56.12%; 6.36%.

*Synthesis of* $[(C_5Me_5)_2Th]_2(\mu_2\text{-}AsMes)_2$, **7**. A 5 mL, colorless, $Et_2O$ solution of $H_2AsMes$ (102 mg, 0.520 mmol) was added dropwise to a stirring, 4 mL, colorless solution of $(C_5Me_5)_2ThMe_2$ (277 mg, 0.520 mmol) at room temperature. The mixture became golden yellow over the course of the addition, then orange, then orange-red over the following 20 min. The mixture was then left to stir for the night, and by the morning it had become dark orange/red. The mixture was filtered through diatomaceous earth and concentrated to ∼2 mL, then cooled to −30 °C to facilitate crystallization. By 30 min, large dark orange-red crystals had formed, which were isolated, triturated in ∼3 mL of pentane, and then isolated and dried again, leaving a dark orange-brown powder, 145 mg, 40%. Crystals suitable for X-ray diffraction were grown from a concentrated $Et_2O$ solution at −30 °C. $^1$H NMR ($C_6D_6$, 600 MHz, 25 °C): $\delta$ 7.18 (s, 4H, *m*-H), 2.67 (s, 12 H, *o*-$CH_3$), 2.46 (s, 6H, *p*-$CH_3$), 2.21 (s, 30H, $C_5Me_5$). $^{13}$C{$^1$H} NMR ($C_6D_6$, 150 MHz, 25 °C): $\delta$ 155.93 (s, *i*-$C_{aryl}$), 140.78 (s, *o*-$CH_3$), 132.84 (s, *p*-$CH_3$), 127.84 (s, $C_5Me_5$), 127.36 (*m*-$C_{aryl}$), 30.87 (s, *o*-$CH_3$), 20.92 (s, *p*-$CH_3$), 14.27 (s, ($C_5Me_5$). IR ($cm^{-1}$): 2958 (s), 2909 (s), 2857 (s), 2722 (w), 2369 (w), 2308 (w), 2090 (w), 1627 (w), 1599 (w), 1447 (m), 1377 (m), 1261 (m), 1085 (m), 1018 (s), 846 (w), 803 (w), 803 (w), 617 (w). Elemental analysis calculated for $C_{58}H_{82}As_2Th_2$ (1393.19 g/mol): C, 50.00%; H, 5.93%. Found: C, 50.25%; 5.67%.

*Synthesis of* $[(C_5Me_5)_2U]_2(\mu_2\text{-}AsMes)_2$, **8**. A 20 mL scintillation vial was charged with $(C_5Me_5)_2UMe_2$ (130 mg, 0.241 mmol) and 6 mL of toluene. The dark orange solution was cooled to −30 °C in a glovebox freezer, and the $H_2AsMes$ (47 mg, 0.240 mmol) was added dropwise as a 3 mL, colorless toluene solution. The mixture was allowed to warm to ambient temperature, and in ∼30 min, it had noticeably darkened. By the morning, the mixture had become dark brown/black, and it was filtered through diatomaceous earth, then concentrated to a black solid under vacuum. The residue was triturated in 3 mL of pentane, then isolated and dried under vacuum, leaving a black, analytically pure, microcrystalline solid, 109 mg, 64%. Crystals suitable for X-ray diffraction were grown from a concentrated $Et_2O$ solution at −30 °C. $^1$H NMR ($C_6D_6$, 600 MHz, 25 °C): $\delta$ 10.17 (s, 60 H, ($C_5Me_5$), 5.15 (s, 6 H, *p*-$CH_3$), −4.59 (s, 4 H, *m*-H), −65.7 (s, 12H, *o*-$CH_3$). IR ($cm^{-1}$): 2954 (s), 2883 (s), 2856 (s), 2719 (w), 2091 (w), 1626 (w), 1598 (w), 1449 (s), 1377 (m), 1267 (w), 1261 (w), 1174 (w), 1095 (w), 1017 (m), 945 (w), 846 (m), 803 (w), 706 (w), 602 (w). Elemental Analysis calculated for $C_{58}H_{82}As_2U_2$ (1405.17 g/mol): C, 49.58%; H, 5.88%; Found: C, 49.94%; 5.72%.

*Synthesis of* $\{(C_5Me_5)_2Th[\mu_2\text{-}P(H)(2,4\text{-}Me_2C_6H_2\text{-}6\text{-}CH_2)]\}_2$, **9**. *Method A*. A 10 mL toluene solution of $(C_5Me_5)_2ThMe_2$ and $H_2PMes$ was heated with stirring in a sealed flask to 60 °C for 1 h. The mixture became yellow-orange. The mixture was cooled to room temperature, and the volatiles were removed under vacuum. The yellow/orange residue was extracted in 4 mL of $Et_2O$ twice, filtered through diatomaceous earth, reduced to ∼2 mL under vacuum, and then cooled to −40 °C to facilitate crystallization. After a second recrystallization from $Et_2O$, a crop of yellow crystals was recovered, 161 mg, 66%. The $^1$H NMR spectrum of **9** exhibited a resonance consistent with the $(C_5Me_5)^-$ ligands at 1.89 ppm, as well as resonances indicative of methyl and methylene groups integrating to 6 and 4H, respectively, at 0.12 and −0.19, a doublet for the P−H bonds ($^1J_{P-H}$ = 235 Hz), and a single resonance corresponding to four aryl protons at 6.94, but additional resonances indicative of a mixture of products were also visible. $^{31}$P{$^1$H} NMR ($C_6D_6$, 101 MHz, 25 °C): $\delta$ (ppm) −33.54 (s). $^{31}$P NMR ($C_6D_6$, 101 MHz, 25 °C): $\delta$ (ppm) −33.54 (d, $^1J_{P-H}$ = 192 Hz).

*Method B*. A 2 mL $C_6D_6$ solution of $(C_5Me_5)_2ThMe(I)$ (50 mg, 0.078 mmol) was added to KP(H)Mes (15 mg, 0.079 mmol), resulting in a cloudy mixture that immediately turned orange. The mixture was transferred to a J. Young tube and shaken vigorously for 5 min. The $^1$H, $^{31}$P{$^1$H}, and $^{31}$P NMR spectra were collected at 10 min of total reaction time, indicating conversion to a mixture of the previously published $(C_5Me_5)_2Th[P(H)Mes]_2$,[25] and **9** in an approximate 1:5 ratio.

*Synthesis of* $[(C_5Me_5)_2U(\mu_2\text{-}PMes)]_2$, **10**. A 3 mL toluene solution of $H_2PMes$ (332 mg, 2.18 mmol) was added dropwise to a stirring, 5 mL toluene solution of $(C_5Me_5)_2UMe_2$ (1.174 g, 2.18 mmol). The mixture was allowed to stir for 18 h and then filtered through diatomaceous earth, and the volatiles were removed under vacuum. The resulting black solid was triturated in pentane, resulting in a microcrystalline suspension that was collected over a medium-porosity fritted glass funnel. The resulting black solid was washed with 4 mL of cold (−40 °C) pentane twice, leaving a microcrystalline black solid, 1.07 g, 74%. $^1$H NMR ($C_6D_6$, 600 MHz, 25 °C): $\delta$ 10.65 (s, 30H, $C_5Me_5$), 5.63 (s, 6H, *p*-$CH_3$), −4.80 (s, 4H, *m*-H), −74.3 (s, 12H, *o*-H). IR ($cm^{-1}$): 2955 (s), 2909 (s), 2884 (s), 2854 (s), 2718 (w), 2299 (w), 1475 (w), 1449 (s), 1376 (m), 1260 (w), 1173 (w), 1081 (w), 1034 (m), 1020 (m), 947 (w), 847 (m), 803 (w), 711 (w), 605 (w). Elemental Analysis calculated for $C_{58}H_{82}P_2U_2$ (1317.27 g/mol): C, 52.88%; H, 6.27%. Found: C, 52.54%; 6.09%.


https://doi.org/10.1021/acs.inorgchem.1c01256
Inorg. Chem. 2021, 60, 10614−10630

*Synthesis of [(C$_5$Me$_5$)$_2$Th]$_2$(μ$_2$-AsMes)(μ$_2$-O), **11**.* A 100 mL Strauss flask was charged with a 10 mL toluene solution of **7** (175 mg, 0.126 mmol), and the $OPPh_3$ (70 mg, 0.252 mmol) was added dropwise, as a 5 mL solution in toluene. The flask was sealed, and the mixture was heated to 70 °C for 2 h, during which the color changed from dark orange/brown to dark red-orange/red). The flask was allowed to cool to room temperature and brought into a glovebox, and the solution was filtered through diatomaceous earth, then concentrated to a dark red-brown solid. The solid residue was recrystallized twice from $Et_2O$, affording red crystals, 115 mg, 75%. Crystals suitable for X-ray diffraction were grown at −40 °C from a concentrated solution in tetrahydrofuran (THF). $^1$H NMR ($C_6D_6$, 600 MHz, 25 °C): δ (ppm) 7.22 (s, 2H, *m*-H), 2.80 (s, 6H, *o*-$CH_3$), 2.39 (s, 3H, *p*-$CH_3$), 2.13 (s, 60H, ($C_5Me_5$). $^{13}$C{$^1$H} NMR ($C_6D_6$, 150 MHz): δ (ppm) 153.96 (s, *o*-C), 140.89 (s, *i*-C), 133.02 (s, *p*-C), 128.34 (s, *m*-C), 126.54−125.54 (m, $C_5Me_5$), 28.55 (s, *o*-$CH_3$), 21.09 (s, *p*-$CH_3$), 13.17 (s, ($C_5Me_5$)). IR (cm$^{-1}$): 2962 (s), 2907 (s), 2858 (s), 2723 (w), 2279 (w), 2903 (w), 1627 (w), 1599 (w), 1439 (m), 1384 (m), 1261 (m), 1092 (m), 1020 (s), 846 (m), 617 (m), 519 (m). Elemental Analysis calculated for $C_{49}H_{71}OAsTh_2$ (1215.08 g/mol): C, 48.44%; H, 5.89%. Found: C, 48.79%; 6.07%.

*Synthesis of [(C$_5$Me$_5$)$_2$U(η$^2$-As$_2$Mes$_2$)][(C$_5$Me$_5$)$_2$U(OPPh$_3$)$_2$], **12**.* A 4 mL toluene solution of $OPPh_3$ (60 mg, 0.216 mmol) was added dropwise to a stirring, 3 mL, toluene solution of **8** (151 mg, 0.107 mmol) at room temperature. The mixture was allowed to stir for 18 h, then filtered through diatomaceous earth, and the volatiles were removed under vacuum, leaving 180 mg of a brown/black solid. Attempts were made to crystallize the resulting black residue from a wide range of organic solvents, but the product would nearly always precipitate as an oil. A small number of black crystals was grown from $Et_2O$ at −40 °C, only once, which were suitable for X-ray diffraction. $^{31}$P{$^1$H} ($C_6D_6$, 121 MHz, 25 °C): δ 86.97 (s, $OPPh_3$).

*Synthesis of (C$_5$Me$_5$)$_2$U(=PMes)OPPh$_3$, **13**.* Solid $OPPh_3$ (253 mg, 0.909 mmol) was added portionwise to a stirring, 8 mL toluene solution of **10** (600 mg, 0.455 mmol) at room temperature. The mixture was stirred for 45 h at room temperature, then filtered through diatomaceous earth, and the volatiles were removed under vacuum, leaving a dark red/brown solid. The solid was recrystallized twice from $Et_2O$ at −40 °C, 399 mg, 47%. $^1$H NMR ($C_6D_6$, 600 MHz, 25 °C): δ 22.89 (s, 2H, Mes-H), 22.71 (s, 3H, *p*-$CH_3$), 15.62 (s, 6H, *o*-$CH_3$), 4.20 (t, 3H, $^3J_{H-H}$ = 7.80 Hz, $OPPh_3$ *p*-H), 2.52 (s, 6H, $OPPh_3$ *m*-H), 1.957 (s, 30H, $C_5Me_5$), −13.22 (s, br, 6H, $OPPh_3$ *o*-H). $^{31}$P{$^1$H} NMR ($C_6D_6$, 110 MHz, 25 °C): δ 12.56. IR (cm$^{-1}$): 3055 (s), 2964 (s), 2898 (s), 2854 (s), 2715 (w), 2329 (w), 1590 (w), 1468 (w), 1454 (w), 1438 (s), 1373 (w), 1160 (w), 1124 (s), 1122 (s), 1078 (s), 1047 (w), 1025 (w), 997 (w), 750 (m), 720 (m), 695 (m), 626 (w), 541 (s). Elemental Analysis calculated for $C_{47}H_{56}OP_2U$ (936.92 g/mol): C, 60.25%; H, 6.02%; Found: C, 60.48%; 6.15%.

**Electrochemistry.** Cyclic voltammetry (CV) experiments were conducted using a CH Instruments (CHI) model 700D series workstation, and the data were analyzed using CHI software version 12.05. All experiments were conducted inside a $N_2$ atmosphere glovebox with an electrochemical cell consisting of a 10 mL vial, Pt disc electrode (3 mm diameter), a platinum wire counter electrode, and a silver wire plated with AgCl as a quasi-reference electrode. The working electrode surfaces were polished prior to each set of experiments and were periodically replaced to prevent a buildup of oxidized or reduced products on the electrode surfaces. Solutions employed during CV studies had concentrations of 1.0−1.5 mM in analyte and 100 mM in tetrabutylammonium tetrakis(pentafluorophenyl)borate as the supporting electrolyte. Potentials were reported versus decamethylferrocene, which was added as an internal standard for calibration at the end of each experiment. Decamethylferrocene was separately referenced to ferrocene (0 V), under the same conditions. The initial scan polarity was negative for all measurements. Scan-rate dependence experiments were performed at 500, 250, 100, and 50 mV/s. All data were collected in a positive-feedback IR compensation mode to minimize the uncompensated resistance in the solution cells. The THF solution cell resistances were measured prior to each run to ensure resistances were ∼1600 Ω or less.

**Magnetic Measurements.** Magnetic susceptibility data were collected using Quantum Design PPMS (for **6**, **8**, **10**, **13**) or MPMS3 (for **4**) instruments; the physical property measurement system (PPMS) employed a vibrating sample module. All sample manipulations were performed inside a dinitrogen-filled glovebox (MBRAUN Labmaster 130). Samples measured on the PPMS used finely ground polycrystalline samples that were loaded into sample holders sourced from Quantum Design, where the outer casing was sealed with eicosane wax. Samples measured on the MPMS used finely ground polycrystalline samples that were loaded into polyethylene bags and sealed in the glovebox, and then the bags were inserted into a drinking straw and inserted into the instrument. Ferromagnetic impurities were checked through a variable field analysis (from 0 to at least 5 kOe) of the magnetization at 100 K; a slight deviation from linearity was noted below 1000 Oe for **4**, **10**, and **13**. Therefore, magnetic susceptibility data were collected at temperatures ranging from 2 to 300 K in the *M* versus *H* linear regime at several measuring fields; for comparison, all data shown in the Results Section are reported with a 5 kOe measuring field; data for other fields are collected in the Supporting Information. Data were corrected for the magnetization of the sample holder by subtracting the susceptibility of an empty container and for the diamagnetic contributions of the sample by using Pascal's constants.[56]

**Computational Details.** Structural optimizations were performed on phosphido, arsenido, diphosphido, diarsenido, phosphinidene, phosphinidiide, and arsinidiide complexes of U(IV) and Th(IV) utilizing the PBE0[57,58] density functional along with the def-TZVP basis set;[59] a 60-electron effective core potential was applied to both thorium and uranium centers.[60−62] Apart from the dinuclear open-shell U(IV) arsinidiide and phosphinidiide complexes, energetic minima were verified by a harmonic frequency analysis. In the case of outstanding complexes, the frequency analysis revealed imaginary frequencies of ∼*i*20 cm$^{-1}$, which could not be eliminated despite repeated attempts. An inspection of the corresponding mode revealed them to be associated with the rotation of peripheral methyl groups, indicating that the nonoptimal structures were suitable for use in the investigation of metal−ligand bond characterization. All DFT calculations were conducted utilizing the Turbomole V6.6 software package;[63] orbital analysis was conducted utilizing NBO6,[64] schematic production was performed using the GaussView 5.0 visualization package,[65] and QTAIM analysis was performed within the AIMAll V19.02.13 software suite.[66]

## RESULTS AND DISCUSSION

Complexes **1**, $(C_5Me_5)_2Th[As(H)Mes]_2$, and **2**, $(C_5Me_5)_2U[As(H)Mes]_2$, were prepared via protonolysis reactions between $(C_5Me_5)_2AnMe_2$ and 2 equiv of $H_2AsMes$ and isolated in yields of 79% and 80% for **1** and **2**, respectively, eq 1. The resonances of

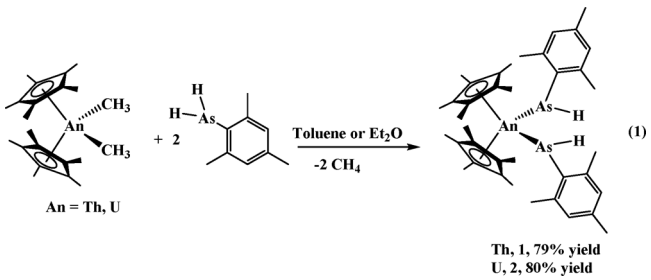


(1)

**1** in the $^1$H NMR spectrum span the typical diamagnetic range, with the As−H resonance at 2.51 ppm, slightly upfield with respect to that of $(C_5Me_5)_2Th[As(H)Tipp]_2$, Tipp = 2,4,6-$^i$Pr$_3$C$_6$H$_2$,[25] at 2.61 ppm. Complex **2** exhibits broadened and paramagnetically shifted resonances in the $^1$H NMR spectrum characteristic of a U(IV) species. The chemical shift of the As−H resonance in **2** at −151.1 ppm is upfield compared to that reported for $[U(Tren^{TIPS})(AsH_2)]$[23] at −131.4 ppm as well as the −122.9 ppm for the P−H resonance in $(C_5Me_5)_2U$-


https://doi.org/10.1021/acs.inorgchem.1c01256
Inorg. Chem. 2021, 60, 10614−10630

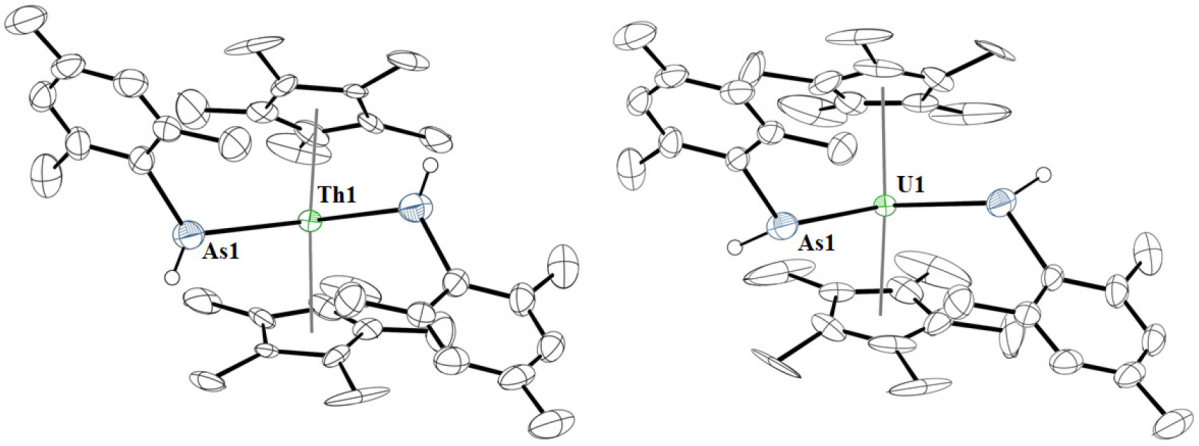


**Figure 1.** Thermal ellipsoid plots of **1** (left) and **2** (right) are shown at the 50% probability level. Hydrogen atoms were omitted for clarity, with the exception of those bound to the arsenic atoms. Pertinent structural information is as follows: Th1−As1, 2.9942(7) Å; As1−Th1−As1, 103.48(3)°; U1−As1, 2.9087(5) Å; As1−U1−As1, 100.61(2)°.

$[P(H)Mes]_2$.[67] Both **1** and **2** have IR absorptions at 2090 and 2093 $cm^{-1}$, respectively, that are attributed to the As−H bond stretching mode.[23]

The solid-state structures of **1** and **2** were determined using an X-ray crystallographic analysis, Figure 1. The Th−As bond distance of 2.9942(7) Å is very close to that of $(C_5Me_5)_2$Th-[As(H)Tipp]$_2$,[25] at 3.0028(6) Å, and the arsenido moiety in $[\{(C_5Me_5)_2Th[\mu_2\text{-As(H)Tip}](\mu_2\text{-AsTipp})\}K]_2$ at 3.0860(4) Å.[30] The structural characteristics of **1** are similar to those of the previously reported Th-arsenido complexes[27] bearing ancillary triamidosilylamine (Tren) ligands, [Th(Tren$^{TIPS}$)-$(AsH_2)$], [Th(Tren$^{TIPS}$){As(SiMe$_3$)$_2$}], and [Th(Tren$^{DMBS}$)-{As(SiMe$_3$)$_2$}], at 3.065(3), 2.956(9), and 3.0456(9) Å, respectively. Complex **1** also bears some similarity to the arsenido-cluster-bridged $[(1,3\text{-}^tBu_2C_6H_3)_2Th]_2(\mu_2\text{-}\eta^{2:1:2:1}\text{-}As_6)$ complex reported by the Scherer group,[31] which exhibited Th−

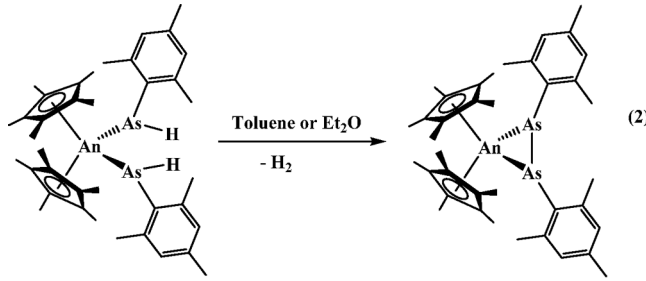


As bond distances of 2.930(3), 3.018(2), 3.040(2), 3.044(2), 3.005, and 2.913(2) Å. Complex **2** exhibits a U−As bond length of 2.9087(5) Å, which is shorter than that in [U(Tren$^{TIPS}$)-$(AsH_2)$],[23] with a U−As bond distance of 3.004(4) Å, and

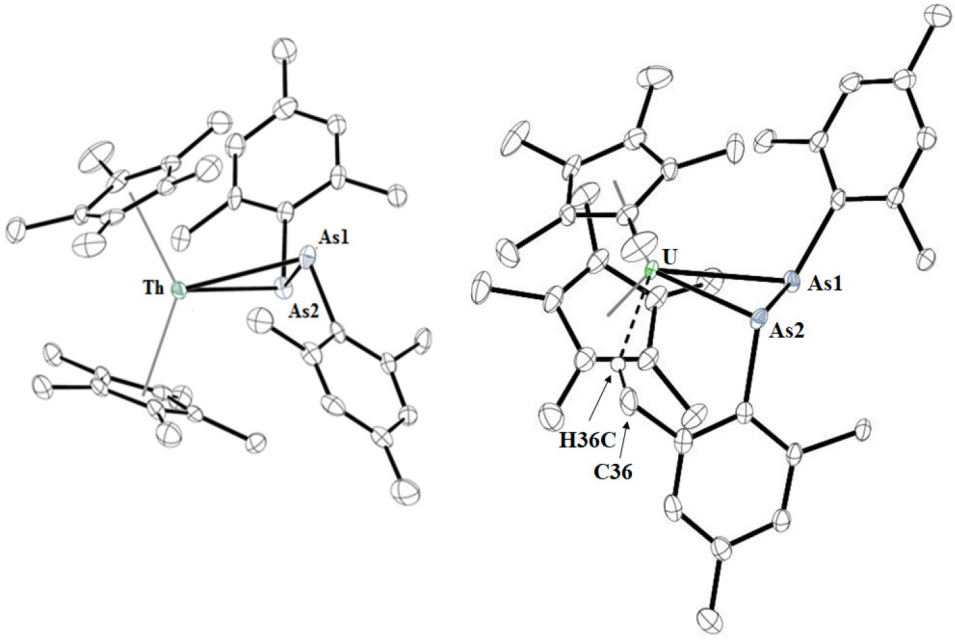


**Figure 2.** Thermal ellipsoid plots of **3** (left) and **4** (right) are shown at the 50% probability level. Hydrogen atoms were omitted for clarity. Pertinent bond distances and angles are as follows: Th1−As1, 2.923(2) Å; Th1−As2, 2.971(3) Å; As1−As2, 2.4454(7) Å; As1−Th−As2, 49.01(4)°; U1−As1, 2.9231(9) Å; U1−As2, 2.8914(11) Å; As1−As2, 2.4320(3) Å; As1−U−As2, 49.326(18)°.


https://doi.org/10.1021/acs.inorgchem.1c01256
Inorg. Chem. 2021, 60, 10614−10630

within the range of the asymmetric bond distances of $[\{U(Tren^{TIPS})\}_2(\mu\text{-As})]$[68] at 2.943(4) and 2.889(4) Å. The structural characteristics of **2** are also similar to those of the previously reported U-arsenido complexes[27] of 2.942(9) and 2.9062(7) Å for the complexes bound by $Tren^{DMBS}$ and $Tren^{TIPS}$, respectively.

Both **1** and **2** exhibit thermal instability at room temperature, gradually eliminating 1 equiv of $H_2$ (as observed by $^1$H NMR spectroscopy) and coupling the arsenido moieties, forming the diarsenido species $(C_5Me_5)_2An(\eta^2\text{-}As_2Mes_2)$, An = Th, **3**; U, **4**, eq 2. Likely as a consequence of the steric bulk at the *ortho*-positions on the aryl rings, $(C_5Me_5)Th[As(H)Tipp]_2$[25] did not exhibit thermal decomposition to a diarsenido complex even after being stirred for extended periods of time at room temperature. Beginning with **1**, conversion to **3** is completed over 12−16 h when stirred in either $Et_2O$ or toluene, with an accompanying color change of deep orange to dark green. The $^1$H NMR spectrum of **3** showed the $(C_5Me_5)^{1-}$ methyl resonances for both **1** and **3** are nearly identical and that the resonances for the ring protons and *ortho*/*para* methyl groups in **3** deviate only slightly from those of **1**. The $(C_5Me_5)^{1-}$ methyl resonance for **4** exhibited a large upfield shift to 7.47 ppm, compared to that of **2** at 15.57 ppm. Apart from that for the *para*-methyl groups in **4**, the resonances for the aryl protons and methyl groups on the rings in **4** are unobservable across the range of temperatures examined, from −40 to 60 °C.

The structures of **3** and **4** were determined by an X-ray crystallography analysis, Figure 2. These, and similar moieties,[15,69] often take the form of anionic clusters containing As−As bonds and are more commonly encountered in transition-metal chemistry.[70−76] Several carborane-type anionic ligands incorporating diarsenido-type fragments have also been

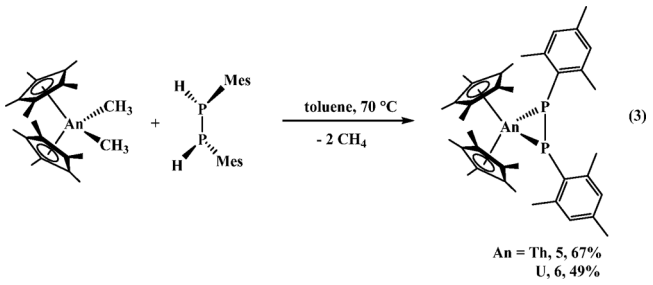


(3)

reported.[77−82] The Th−As bond distances of 2.923(2) and 2.971(3) Å and the U−As bond lengths of 2.9231(9) and 2.8994(7) Å are slightly shorter than those observed in **1** and **2**, respectively. The As−As bond lengths of 2.4454(7) Å in **3** and 2.4320(3) Å in **4** are consistent with the As−As bond distances of 2.472(3) Å in $Mes_2AsAsMes_2$[83] as well as 2.4572(3) Å in $(C_5H_5)_2Ti(\eta^2\text{-}As_2Tipp_2)$.[84] Complexes **3** and **4** bear a similarity to the Liddle group's bridging $(HAsAsH)^{2-}$ complex, $[U(Tren^{TIPS})]_2(\mu_2{:}\eta^2\text{-}As_2H_2)$,[24] with U−As bond distances at 3.1203(7) and 3.1273(7) Å, a significant increase in bond length due to the steric demand of the $Tren^{TIPS}$ ligand. For comparison, the As−As bond distance in $[U(Tren^{TIPS})]_2(\mu_2{,}\eta^2\text{-}As_2H_2)$ is 2.1402(13) Å, much shorter than those in **3** and **4**. The An−As1-C(ipso) bond angles are 99.18(14)° and 111.53(14)° for **3** and 96.70(7)° and 111.13(7)° for **4**. Complex **4** exhibits anagostic interactions[85] from the *o*-$CH_3$ groups on one of the mesityl rings in each case, with a U−H36C distance of ∼2.55 Å. This is contrast to the thorium analogue **3**, whose closest Th−H contact is ∼2.80 Å.

In contrast to the bis(arsenido) complexes, the bis(phosphido) complexes are more thermally stable. Heating

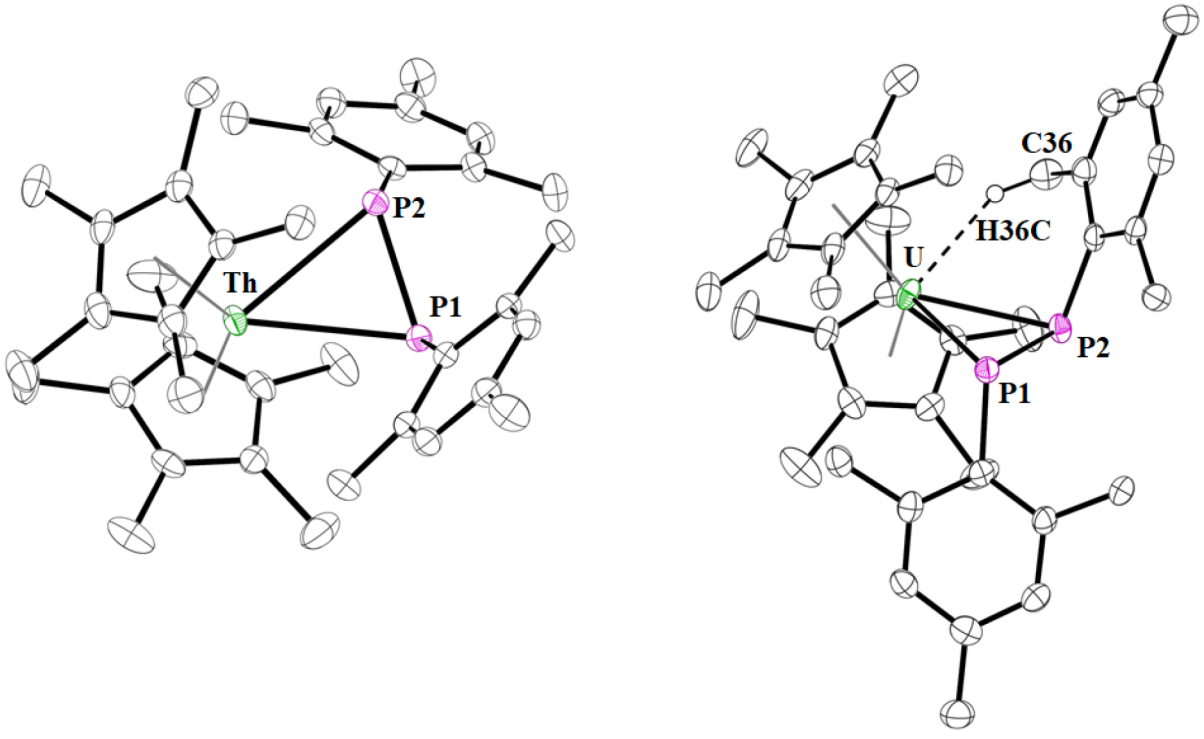


**Figure 3.** Thermal ellipsoid plots of **5** (left) and **6** (right) are shown at the 50% probability level. Hydrogen atoms were omitted for clarity, with the exception of the methyl group participating in the anagostic interaction in **6**. Pertinent bond distances and angles are as follows: Th1−P1, 2.8463(7) Å; Th1−P2, 2.8322(6) Å; P1−P2, 2.1953(8) Å; P1−Th−P2, 45.486(18)°; U1−P1, 2.7799(10) Å; U1−P2, 2.7903(10) Å; U1−H36C, 2.545 Å; P1−P2, 2.1825(13) Å; P1−U−P2, 46.13(3)°.



https://doi.org/10.1021/acs.inorgchem.1c01256
*Inorg. Chem.* 2021, 60, 10614−10630

$(C_5Me_5)_2An[P(H)Mes]_2$[25,67] to 100 °C in toluene does not form the diphosphido complexes or lead to decomposition. This contrasts to the reactivity of $(1,3\text{-}^tBu_2C_5H_3)_2Th[P(H)Tipp]_2$, which produces the diphosphido moiety upon heating to 75 °C.[39] An alternate route to the diphosphido complexes was used with the reaction of $(C_5Me_5)_2An(CH_3)_2$ with dimesityldiphosphane, MesP(H)P(H)Mes,[53] eq 3. At room temperature, no reaction takes place, but heating to 70 °C afforded the desired diphosphido complexes, $(C_5Me_5)_2An(\eta^2\text{-}P_2Mes_2)$, An = Th, **5**; U, **6**. While the uranium complex reacts immediately with the diphosphane at an elevated temperature, the reaction with thorium took several hours to reach completion. This is presumably due to the higher effective nuclear charge of uranium, making the methyl groups more basic when coordinated to uranium versus thorium. These differences in reactivity of dialkyl thorium and uranium complexes have been previously observed.[86] Complex **5** is dark green, while **6** is black in color, similar to their diarsenido counterparts. The $^{31}P$ NMR spectrum of **5** exhibits a resonance at 58.92 ppm, downfield from that of the Hohloch group's recently reported[87] $(PN)_2La(\eta^2\text{-}P_2Mes_2)$, PN = $[\kappa^2\text{-}^iPr_2PN(Mes)]^{1-}$, at 30.5 ppm, but similar to the resonance at 55.3 ppm in $(C_5Me_5)_2Th(\kappa^2\text{-}P_3Ph_3)$,[88] and in between those of 81.9 and 14.4 ppm for $(1,3\text{-}^tBu_2C_6H_3)_2Th(\eta^2\text{-}P_2Tipp_2)$ and $(1,3\text{-}^tBu_2C_6H_3)_2Th(\eta^2\text{-}P_2Tipp_2)$(DMAP) (DMAP = 4-dimethylaminopyridine),[39] respectively. The $^{31}P$ NMR resonance at 58.92 ppm for **5** can also be compared to those of the $(C_5Me_5)_2Zr(\eta^2\text{-}P_2Mes_2)$[89] and $[C_5H_2(SiMe_3)_2]_2Hf(\eta^2\text{-}P_2Ph_2)$[90] counterparts, which have significant downfield shifts of 134.9 and 193.22 ppm, respectively. This shift indicates more covalent character in the Group IV phosphorus bond rather than for the f elements (Th and La), which supports the conclusions drawn from X-ray absorption spectroscopy measurements on metallocene transition metal and actinide complexes.[91]

Complexes **5** and **6** were also structurally characterized using X-ray crystallography, Figure 3. The An-P bond distances are 2.8463(7) and 2.8322(6) Å in **5** and 2.7799(10) and 2.7903(10) Å in **6**. These distances for **5** are in between the 2.778(1) and 2.934(1) Å values observed in $(1,3\text{-}^tBu_2C_6H_3)_2Th(\eta^2\text{-}P_2Tipp_2)$-(DMAP). The P-An-P angles can be compared to that of $(1,3\text{-}^tBu_2C_6H_3)_2Th(\eta^2\text{-}P_2Tipp_2)$(DMAP), which has a P−Th−P bond angle of 44.5(1)°,[39] smaller than the P-An-P angles of 45.486(18) and 46.13(3)° in **5** and **6**, respectively. The identical Zr(IV) structure, $(C_5Me_5)_2Zr(\eta^2\text{-}P_2Mes_2)$, has a P−Zr−P angle of 48.65(9)°.[89] The P−P bond distances in **5** and **6** of 2.1953(8) and 2.1825(13) Å, respectively, are consistent with those found for the Ar = Tipp (2.1699(5) Å) and Ar = 2,6-$^iPr_2C_6H_3$ (2.1826(7) Å) variants of $(C_5H_5)_2Ti(\eta^2\text{-}P_2Ar_2)$ complexes.[92] As observed in the uranium diarsenido, **4**, the uranium diphosphido, **6**, also displays anagostic interactions. The U1−H36C distance is 2.545 Å with a U−H36C-C36 angle of 147.9°. In contrast to the diarsenido complexes, **5** does contain a Th−H29A contact of ∼2.672 Å. In the case of **4** and **6**, we surmise the shorter U-E bonds, relative to the Th-E bond distances, forces the methyl groups closer to the metal center, allowing for the anagostic interactions.

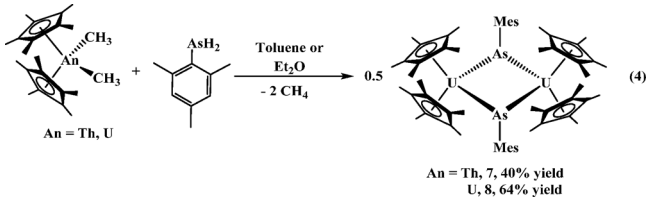

(4)

The reaction of 1 equiv of $H_2AsMes$ with $(C_5Me_5)_2AnMe_2$ (An = Th, U) in diethyl ether or toluene, stirred for ∼12−16 h at room temperature, results in the formation of complexes **7** and **8** in average yields of ∼40, and 64%, respectively, eq 4. The chemical shifts for **7** in the $^1H$ NMR spectrum are similar to those of **1**, except for the lack of an As−H resonance. The $^1H$ NMR spectrum of **8** shows the expected paramagnetic character, with the resonance for the *o*-$CH_3$ groups appearing at −65.7 ppm, a stark contrast from that of **2** at −24.30 ppm. The $(C_5Me_5)^{1-}$ resonances for **2** and **8** appear at 15.43 and 10.17 ppm, respectively, reflecting a similar upfield shift.

The structures of **7** and **8** were also determined by an X-ray crystallography analysis, Figure 4. The Th−As bond distance of 2.8787(6) Å in **7** is longer than the arsinidiide bond distance of

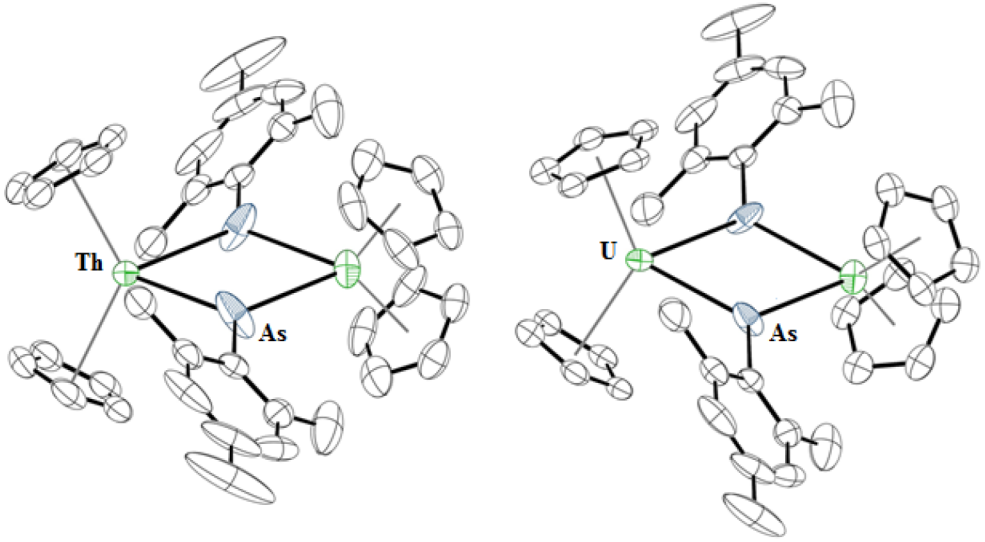


**Figure 4.** Thermal ellipsoid plots of **7** (left) and **8** (right) are shown at the 50% probability level. Hydrogen atoms and cyclopentadienyl methyl groups were omitted for clarity. Pertinent bond distances and angles are as follows: Th−As, 2.8787(6) Å; As−Th−As, 71.516(4)°; U−As, 2.8310(4) Å; As−U−As, 69.808(19)°.


https://doi.org/10.1021/acs.inorgchem.1c01256
Inorg. Chem. 2021, 60, 10614−10630

2.7994(4) Å in $[\{(C_5Me_5)_2Th[\mu_2\text{-}As(H)Tipp](\mu_2\text{-}AsTipp)\}K]_2$, 2.8565(7) Å in $Th(Tren^{TIPS})(\mu_2\text{-}AsH)K(15C5)$, 15C5 = 15-crown-5, and $\{Th(Tren^{TIPS})\}_2(\mu\text{-}As)][K(15C5)_2$[27] at 2.8063(14) and 2.8060(14) Å. The U−As bond length of 2.8310(4) Å is much longer than the terminal arsinidene $[U(Tren^{TIPS})(AsH)]^{1-}$ bond distance of 2.7159(13) Å as well as the 2.74(1) Å in the arsinidiide $[U(Tren^{TIPS})(AsH)K(2.2.2\text{-cryptand})]$.[23] However, these distances are significantly shorter than the corresponding An-As distances in **1**, 2.9953(7) Å, and **2**, 2.9087(5) Å.

To make a comparison with phosphorus, the analogous reactions with $(C_5Me_5)_2ThMe_2$ and 1 equiv of $H_2PMes$ were attempted, eq 5. Heating the reaction to 60 °C was necessary to

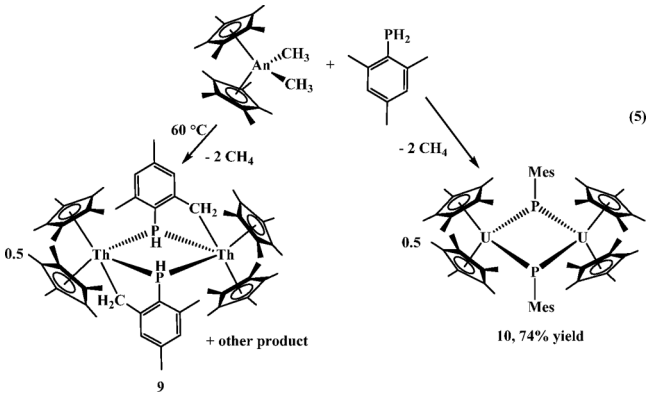


observe a color change from colorless to yellow. However, it was apparent from the $^{31}P\{^1H\}$ NMR spectrum that the phosphinidiide did not form, as a doublet at −33.54 ppm in the $^{31}P$ NMR spectrum was observed, while other thorium phosphinidiide complexes have $^{31}P\{^1H\}$ NMR resonances located downfield of 100 ppm.[41,42] Additionally, the $^{31}P$ NMR spectrum showed a doublet ($^1J_{P-H}$ = 192 Hz) as well as a $\nu_{P-H}$ stretch at 2305 $cm^{-1}$, indicative of a primary phosphido ligand.[93] However, the $^1H$ NMR spectrum exhibited signals indicative of two products, which persisted through multiple recrystallizations, which indicates the reactivity of $(C_5Me_5)_2ThMe_2$ with $H_2PMes$ is relatively more complicated. Efforts to understand this reaction in more detail are currently underway.

The structure was determined by X-ray crystallography to be a dimeric alkyl-phosphido complex, $\{(C_5Me_5)_2Th[\mu_2\text{-}P(H)(2,4\text{-}Me_2C_6H_2\text{-}6\text{-}CH_2)]\}_2$, **9**, the result of a C−H bond activation at the *o*-$CH_3$ of the mesityl ring on the phosphido moiety, Figure 5. An alternate synthetic route was employed in an effort to obtain $[(C_5Me_5)_2Th(\mu_2\text{-}PMes)]_2$, involving the reaction of $(C_5Me_5)_2ThMe(I)$ with KP(H)Mes. The result was again a mixture, this time of **9** as well as the previously reported bis(phosphido) complex, $(C_5Me_5)_2Th[P(H)Mes]_2$, in an approximate 5:1 ratio. This metalation is reminiscent of the proposed mechanism for the formation of the bridging phosphinidiide from reaction of 2 equiv of $(C_5Me_5)_2ThMe_2$ with $H_2P(2,4,6\text{-}^iPr_3C_6H_2)$.[40] In that reaction, transition-state calculations described a P−H activation, followed by a C−H bond activation, similar to the formation of **9**.

The reaction of $(C_5Me_5)_2UMe_2$ with 1 equiv of $H_2PMes$ at room temperature afforded a black solid in good yield (74%). The $^1H$ NMR spectrum showed a resonance at 10.65 ppm for $(C_5Me_5)^{1-}$, similar to the 10.03 ppm signal found for $(C_5Me_5)_2U[P(H)Mes]_2$.[67] With no resonance for the P−H bond observed in the $^{31}P$ NMR or IR spectrum, the X-ray crystallography showed the expected phosphinidiide product, $[(C_5Me_5)_2U(\mu_2\text{-}PMes)]_2$, **10**, Figure 5.

The difference between thorium and uranium is striking. Whether this is due to the 5f orbitals of uranium participating in the bonding to form the phosphinidiide is not known at the present time. We noted in a previous report that the reaction of $(C_5Me_5)_2U[P(H)Mes]_2$ with 2 equiv of $^t$BuCN formed $(C_5Me_5)_2U[\kappa^2\text{-}(N{=}C^tBu)_2P(Mes)]$,[67] which we attributed to

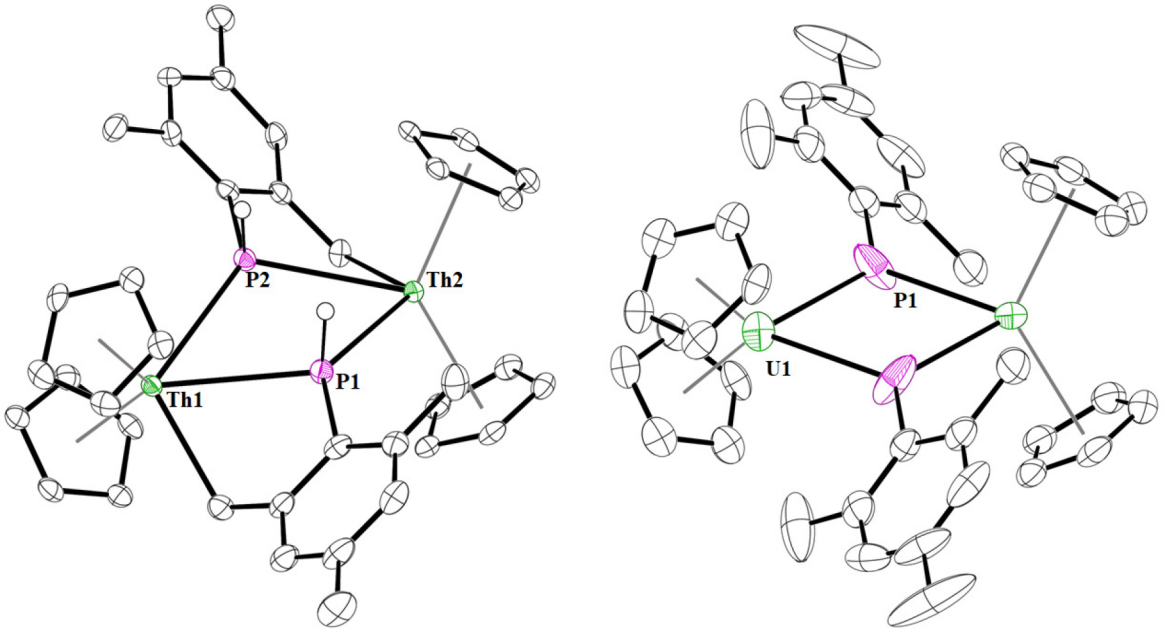


**Figure 5.** Thermal ellipsoid plots of **9** and **10** shown at the 50% probability level. All hydrogens, apart from the phosphido ligands in **9**, and the methyl groups on the $(C_5Me_5)^{1-}$ ligands were omitted for clarity. Selected bond distances and angles: Th1−P1:3.0202(14) Å; Th1−C1:2.541(6) Å; Th1−P2:3.0849(14) Å; Th2−P1:3.0806(14) Å; Th2−P2:3.0364(14) Å; Th2−C10:2.534(5) Å; P1−Th1−P2:58.96(4)°; P1−Th2−P2:58.84(4)°; U1−P1:2.742(3) Å; U1−P1−U1*: 109.72(3)°; P1−U1−P1*: 70.28(2)°.


https://doi.org/10.1021/acs.inorgchem.1c01256
Inorg. Chem. 2021, 60, 10614−10630

the formation of a transient phosphinidene or phosphinidiide. The reaction of **10** with $^{t}$BuCN also forms $(C_5Me_5)_2U[\kappa^2$-$(N{=}C^{t}Bu)_2P(Mes)]$, which supports a phosphinidiide or phosphinidene intermediate, as is the case for zirconium.[94]

Complex **9** has Th1−P bond distances of 3.020(1) and 3.085(1) Å and Th2−P bond lengths of 3.080(1) and 3.036(1) Å. These distances are much longer than the 2.872(5) Å in $(C_5Me_5)_2Th[P(H)Mes]_2$[25] and 2.888(4) Å in $(C_5Me_5)_2Th(Cl)[P(SiMe_3)_2]$.[95] The Th1−C1 and Th2−C10 bond distances are 2.542(5) and 2.533(5) Å, respectively. These Th−C bond lengths are significantly longer than other phosphido-methyl complexes reported, which range from 2.429(5) to 2.473(4) Å.[96,97] This elongation in both Th−P and Th−C bonds is presumably due to the dimeric structure of **9**. Complex **10** is a symmetric dimer in the solid state, with a U−P bond distance of 2.742(3) Å. This is only slightly shorter than the 2.7768(12) Å in $(C_5Me_5)_2U[P(H)Mes]_2$[67] but identical to the 2.743(1) Å for the bridging phosphinidiide, $[(C_5Me_5)_2U(OMe)]_2(\mu_2$-PH).[98]

**Computational Analysis.** Complexes **1**−**8** and **10** were analyzed using a density functional analysis incorporating the PBE0 exchange-correlation functional to compare the amount of covalent bonding in the pnictido, dipnictido, and pnictinidiide complexes. The thorium phosphinidiide, which is not observed experimentally, was modeled after the analogous uranium phosphinidiide, **10**, to make a direct comparison. All bond distances and angles showed excellent agreement (within 0.03 Å and 2°) with the experimentally determined values, Table 1. As would be expected, bond covalency, as indicated by bond length, is more pronounced in U complexes than in the Th analogues. This is more prominent in U−P than in U−As bonds but is suppressed from the pnictido → dipnictido → pnictinidene → pnictidiide complex. The $\rho_{BCP}$ value is small in all cases, indicative of predominantly ionic interactions, Table 2. These densities compare well with those of previously reported thorium and uranium phosphido and arsenido complexes.[27,93,99] The bond ellipticity $\varepsilon$ can be utilized as an indicator of multiple bond character though measuring the deviation of the bond from cylindrical symmetry. For a single or triple bond, $\varepsilon$ should be close to zero, whereas for a double bond, deviations are substantial. Bond ellipticities were typically found to be larger in the U complexes, indicative of a higher multiple bond character, with the exception of the pnictidiide complexes, for which the Th-E bonds had a notably high ellipticity. The ellipticity of the U-E bond in the arsenido complex appears to be anomalous. The delocalization indices (DIs), which quantify the electron sharing between bonded atoms, are typically larger in the U complexes and, in contrast to the $\rho_{BCP}$ values, increase in the order pnictido < dipnictido < pnictidiide. It is worth noting that $\rho_{BCP}$ will only measure $\sigma$-type bond character, whereas DI measures electron sharing through all bonding interactions.

In comparison, $\rho_{BCP}$ is consistently larger in M-P than M-As bonds, with the difference being more pronounced in the U complexes. Bond ellipticities are noticeably larger in the phosphido complexes when compared to the arsenide analogues, whereas values are comparable in the dipnictido and pnictidiide. Delocalization indices indicate that M-E electron sharing is comparable, irrespective of the chemical nature of E, although the general trend is for M-As bonds to exhibit slightly greater electron sharing than M-P bonds. This is suggestive of greater overlap-driven covalency in M-P bonds, and greater energy degeneracy-driven covalency in M-As bonds.

**Cyclic Voltammetry of 8 and 10.** To experimentally compare the donating properties of phosphorus and arsenic ligands, electrochemical measurements were performed on the uranium(IV) arsinidiide, **8**, and phosphinidiide, **10**. While several irreversible features are observed in each cyclic voltammagram (Figures S25 and S26), which are presumably due to ligand-based redox events, one quasi-reversible wave is observed, with $E_{1/2}$ values of −2.316 and −2.358 V, for **8** and **10**, respectively, which is assigned to the $U^{IV/III}$ couple, Figure 6. This is consistent with the lowest unoccupied molecular orbital (LUMO) of **8** and **10**, which are both uranium-based (Figures S27 and S28). The more cathodic potential for the phosphinidiide is expected given the better donating ability, thus stabilizing the U(IV) oxidation state, making it more difficult to reduce. These redox couples can be compared to those of uranium(IV) phospholyl[100] and arsolyl complexes, which showed $E_{1/2}$ values of −1.92 V and −1.89 V,

**Table 1. Calculated and Experimental Bond Distances**[a]

| | calculated M-E (avg) (Å) | | experimental M-E (avg) (Å) | |
|---|---|---|---|---|
| complex | Th | U | Th | U |
| phosphido | 2.888 | 2.774 | 2.888(4)[25] | 2.7768(12)[67] |
| arsenido | 3.013 | 2.935 | **1**, 2.9942(7) | **2**, 2.9087(5) |
| diphosphido | 2.840 | 2.786 | **5**, 2.839(1) | **6**, 2.785(1) |
| diarsinido | 2.962 | 2.933 | **3**, 2.947(3) | **4**, 2.907(1) |
| phosphinidiide | 2.835 | 2.784 | | **10**, 2.742(3) |
| arsinidiide | 2.922 | 2.873 | 7, 2.8787(6) | **8**, 2.8310(4) |
| phosphinidene | 2.548 | 2.499 | | **13**, 2.502(1) |

[a]Values are averaged over M-E bonds (E = P, As).

**Table 2. QTAIM-Derived Bond Metric for M-X Bonds**[a]

| | $\rho_{BCP}$ (au) | | $\nabla^2\rho_{BCP}$ (au) | | $\varepsilon$ (au) | | $H$ (au) | | DI (au) | |
|---|---|---|---|---|---|---|---|---|---|---|
| complex | Th | U | Th | U | Th | U | Th | U | Th | U |
| Phosphido | 0.056 | 0.062 | 0.035 | 0.050 | 0.228 | 0.327 | −0.015 | −0.018 | 0.594 | 0.691 |
| arsenido | 0.050 | 0.054 | 0.021 | 0.027 | 0.129 | 0.076 | −0.013 | −0.015 | 0.584 | 0.655 |
| diphosphido[b] | 0.062 | 0.067 | 0.032 | 0.027 | 0.149 | 0.186 | −0.019 | −0.022 | 0.604 | 0.667 |
| diarsinido[b] | 0.055 | 0.057 | 0.022 | 0.015 | 0.149 | 0.161 | −0.016 | −0.017 | 0.625 | 0.671 |
| phosphinidene | 0.077 | 0.082 | 0.105 | 0.116 | 0.297 | 0.553 | −0.027 | −0.030 | 1.195 | 1.345 |
| (M-O bond) | (0.060 | 0.057 | 0.210 | 0.225 | 0.046 | 0.215 | −0.009 | −0.007 | 0.365 | 0.354) |
| phosphinidiide[b] | 0.060 | 0.062 | 0.040 | 0.047 | 0.332 | 0.206 | −0.017 | −0.018 | 0.657 | 0.731 |
| arsinidiide[b] | 0.055 | 0.056 | 0.034 | 0.040 | 0.336 | 0.215 | −0.015 | −0.016 | 0.662 | 0.734 |

[a]M = Th, U; X = P, As. $\varepsilon$ = bond ellipticity, $H$ = energy density, DI = delocalization index. [b]Only one NBO identified as $\sigma$-type bonding, despite qualitative similarities.



https://doi.org/10.1021/acs.inorgchem.1c01256
Inorg. Chem. 2021, 60, 10614−10630

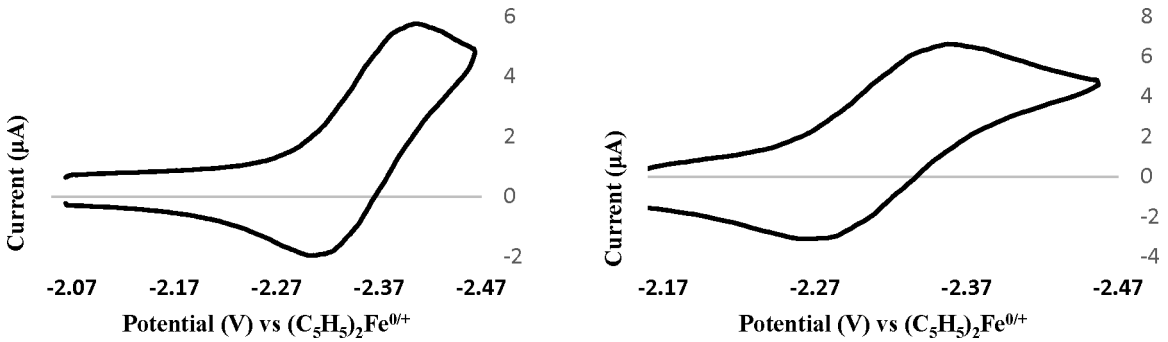


**Figure 6.** Cyclic voltammogram of **10** (left) and **8** (right) for the quasi-reversible region at a scan rate of 0.5 V/s; $E_{1/2}$ = −2.358 V (for **10**) and $E_{1/2}$ = −2.316 V (for **8**).

respectively.[101] The more cathodic potentials for **8** and **10** indicate a greater donation from phosphorus and arsenic in these compounds compared to the phospholyl and arsolyl. While a direct comparison cannot be made, it is noteworthy that the reduction potentials of **8** and **10** are more anodic than those of the imido complexes reported by Kiplinger, $(C_5Me_5)_2U{=}N(2,4,6\text{-}{}^tBu_3C_6H_2)$[102] and $(C_5Me_5)_2U(THF)[{=}N\text{-}(2,6\text{-}{}^iPr_2C_6H_3)]$,[103] which have potentials of −2.61 and −2.40 V, respectively. The difference between the imido and phosphinidiide and arsinidiide complexes is a consequence of the decrease in electronegativity from N to P and the nearly identical electronegativity of P and As,[104] but it also supports the computational results that indicate the differences in bonding between P and As are small. No $U^{V/IV}$ redox couple was observed, as the highest occupied molecular orbital (HOMO) of both **8** and **10** is pnictogen-based, which is attributed to the irreversible nature of observed waves.

**Magnetic Properties of the Uranium-Containing Compounds.** To further characterize the electronic structures of the novel complexes, the magnetic properties of the thermally stable uranium-containing compounds were measured at several temperatures and field strengths. All the complexes show some field dependencies in susceptibility, which may be attributable to trace ferromagnetic impurities and/or mixing of magnetic excited states. For self-consistency, we compare the temperature dependencies of effective magnetic moments for data collected under 5 kOe measuring fields, Figure 7. As found for many U(IV) species, all compounds investigated here show a similar thermal behavior consistent with singlet ground states and a thermal population of magnetic excited states at higher temperatures. The low- and room-temperature $\mu_{eff}$ and $\chi_M T$ values for each compound, scaled on a per-U basis, are collected in Table 3.

When complexes are compared with the same local coordination environments (**4** to **6** and **8** to **10**), pnictogen identity is important to the magnetic response. The As-containing complexes have higher magnetic susceptibilities at temperatures above 50 K compared to the P-containing analogues. For reports of other U-E (E = N/P/As) complexes, the differences in magnetic susceptibilities were attributed to the increased donor strength of P compared to As.[23,105,106] Here, we infer mixed results on relative contributions of the ligand field. Liddle and co-workers have noted that a steeper increase in $\mu_{eff}$ with increasing temperature indicates that the first paramagnetic excited state is at a lower energy and thus more readily occupied.[3] A table of the slopes of the low-temperature $\chi_M T$ versus $T$ data is provided in Table S3 for a qualitative comparison of the energies of the lowest-lying paramagnetic

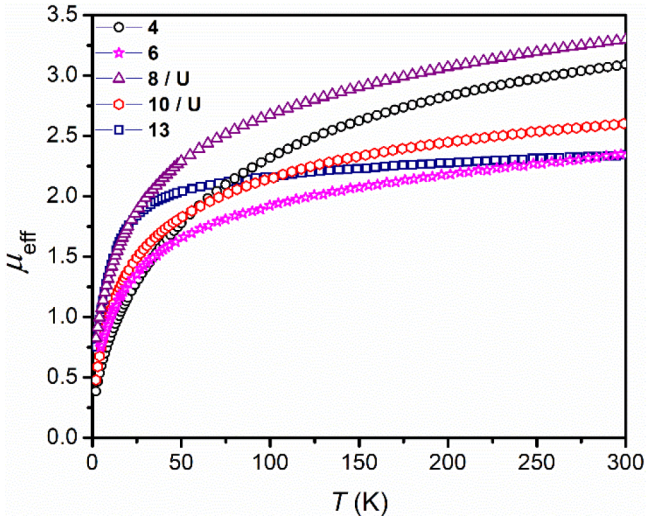


**Figure 7.** Temperature dependence of effective magnetic moment values for compounds **4**, **6**, **8**, **10**, and **13**, measured at 5 kOe; values are scaled per uranium center. The same data plotted as $\chi_M T$ values are collected in Figure S32.

**Table 3. Limiting $\mu_{eff}$ (unitless) and $\chi_M T$ ($cm^3$·K/mol) Values, Measured at 5 kOe**

| compound | $\mu_{eff}$ (5 K) | $\mu_{eff}$ (300 K) | $\chi_M T$ (5 K) | $\chi_M T$ (300 K) |
|---|---|---|---|---|
| **4** | 0.60 | 3.09 | 0.04 | 1.19 |
| **6** | 0.77 | 2.19 | 0.07 | 0.60 |
| **8** (/U) | 1.07 | 3.30 | 0.14 | 1.36 |
| **10** (/U) | 0.75 | 2.60 | 0.07 | 0.85 |
| **13** | 1.06 | 2.34 | 0.16 | 0.69 |

state; we note that the susceptibility data taken in the 2−10 K regime are relatively independent of the measuring field. From the low-temperature magnetic data for diarsenido **4** and diphosphido **6** we can infer that the lowest-lying paramagnetic state in **4** is higher in energy than that in **6**, since the effective magnetic moment of **4** rises more gradually with temperature increase compared to that of **6**; this assignment is also consistent with the fact that the 5 K $\mu_{eff}$ value of **4** is less than that of **6**. In contrast to the mononuclear species, the $\mu_{eff}$ value of As-containing dinuclear complex **8** increases more sharply with temperature increase than what is observed for **10**, suggesting that low-lying paramagnetic states are more accessible for the As-containing analogue. Thus, the relative energies of the first paramagnetic state may vary between As- and P-containing ligands, but that does not contradict the contribution of *multiple*


https://doi.org/10.1021/acs.inorgchem.1c01256
Inorg. Chem. 2021, 60, 10614−10630

paramagnetic excited states at higher temperatures, which seems to be more prevalent for softer As compared to harder P.

When mononuclear and dinuclear species are compared, and with the caveat that arsinidiides and phosphinidiides are quite different from diarsenidos and diphosphidos, respectively, magnetic susceptibilities track higher for the dinuclear species at all temperatures. Given the relative orientations of the U ions from the crystal structures, one might expect bridging orbital orthogonality to lead to ferromagnetic coupling within the various paramagnetic excited states, consistent with the observation of higher effective magnetic moments. While a magnetic exchange coupling between U centers may be operative in both compounds, perturbations in crystal fields manifest in a similar manner to magnetic exchange,[107] making it difficult to deconvolute the effects. Given the similarities in magnetic behaviors relative to other diuranium complexes, it is likely that the differences in magnetic susceptibilities result from crystal field effects.

**Reactivity with $OPPh_3$.** Next, we attempted to separate the dimeric phosphinidiide and arsinidiide complexes of **7**, **8**, and **10** with triphenylphosphine oxide, $OPPh_3$, to prepare the corresponding thorium and uranium arsinidene as well as the uranium phosphinidene complexes. The reaction of **7** with $OPPh_3$, eq 6, exhibited no reaction at room temperature, but

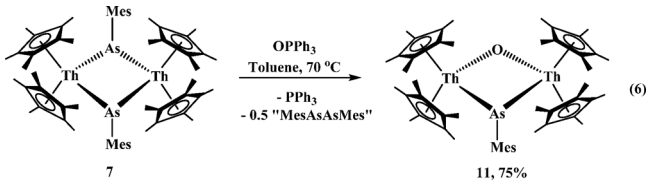

(6)

upon heating to 70 °C, a color change from dark orange-brown to dark red-brown took place. The $(C_5Me_5)^{1-}$ resonance shifted from 2.21 ppm in **7** to 2.13 ppm in the $^1H$ NMR spectrum. Surprisingly, a single resonance in the $^{31}P\{^1H\}$ spectrum at −6 ppm, indicative of free $PPh_3$, was observed. Indeed, the structural characterization showed the product $[(C_5Me_5)_2Th]_2(\mu_2\text{-AsMes})(\mu_2\text{-O})$, **11**, an arsinidiide, oxo bridged dimer, Figure 8. We note that the presumed byproduct, MesAs═AsMes, has not been reported.

This use of $OPPh_3$ as an oxo-delivering agent is rare with f elements. Even Sm(II) and U(III)[108] complexes, known for their reductive chemistry, typically only coordinate $OPPh_3$[109,110] due to the P−O bond strength. For this reason, the conversion of $OPPh_3$ to $PPh_3$ is rare[111] and has been of interest electrochemically.[112−114] The formation of **11** demonstrates the electron-deficient nature of **7** in concert with the oxophilicity of the thorium center. The Th-E-Th bond angles differ significantly with a Th−O−Th angle of 132.0(3)° and Th−As−Th angle of 85.94(3)°. The Th−O bond distances of 2.146(5) and 2.151(5) Å are similar to $[(1,2,4\text{-}^tBu_3C_5H_2)_2Th(\mu_2\text{-O})]_2$, which has an average Th−O bond length of 2.179(2) Å.[115] The Th−As bond distances of 2.8733(10) and 2.8850(10) Å are similar to the 2.8787(6) Å value in the parent arsinidiide, **7**.

The reaction of **8** with $OPPh_3$ was attempted to form the corresponding terminal uranium arsinidene, eq 7, resulting in a black solution. The $^{31}P$ NMR spectrum of the product shows only one singlet resonance at 85.37 ppm. The oily nature hampered the characterization, and while the purity and yield are questionable, a small number of black crystals suitable for X-ray crystallography were isolated only once. The structure was identified via X-ray crystallography as $[(C_5Me_5)_2U(\eta^2\text{-}As_2Mes_2)][(C_5Me_5)_2U(OPPh_3)_2]$, **12**, Figure 9. This product demonstrates that the formation of an As−As bond is sufficient to reduce U(IV) to U(III). We note that a related product, $[(1,3\text{-}^tBu_2C_5H_3)_2U(OPMe_3)_2][1,3\text{-}^tBu_2C_5H_3]$, was recently reported as a minor byproduct from the reduction of U(IV) with KPHMes*, Mes* = 2,4,6-$^tBu_3C_6H_2$.[45]

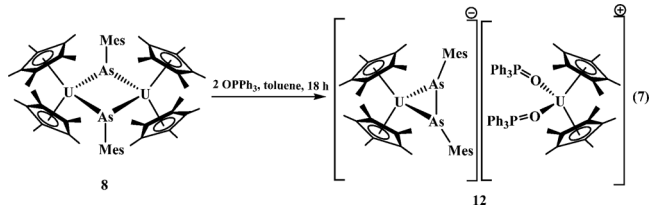

(7)

On the basis of charge balance, **12** is a cation−anion pair of two U(III) complexes with the anion consisting of two $(C_5Me_5)^{1-}$ ligands and one $(MesAsAsMes)^{2-}$, while the cation has two $(C_5Me_5)^{1-}$ and two neutral $OPPh_3$ ligands. The U−As bond distances in **12** are 2.9757(8) and 2.9814(8) Å, which are longer than the 2.9231(9) and 2.8994(7) Å values found in **4**, indicating that **12** contains a more reduced metal center than **4**. The only other U(III)-As bonds, with distances of 2.895(4) and 2.923(4) Å, are in the mixed-valent complex $[U(TrenTIPS)_2(\mu\text{-}\eta^2\text{-(OAs)}:\eta^2\text{-(CAs)-OCAs}]^{1-}$.[68] The U−O distances of 2.361(4) and 2.359(3) Å in **12** are similar compared to those in $[(1,3\text{-}^tBu_2C_5H_3)_2U(OPMe_3)_2][1,3\text{-}^tBu_2C_5H_3]$ of 2.331(5) and 2.348(5) Å.

The reaction of **10** with $OPPh_3$ takes place slowly over time as monitored by $^1H$ and $^{31}P$ NMR spectroscopy, eq 8. Finally, after 45 h, the reaction was complete, during which time the color changed from black to red-brown. One resonance was in the $^{31}P$ NMR spectrum at 12.56 ppm, which was attributed to the $OPPh_3$ coordinating to the uranium center in $(C_5Me_5)_2U(=PMes)(OPPh_3)$, **13**. The isolation of **13** indicates that the P−P bond formation is not sufficient to reduce U(IV) to U(III) to form the analogous product observed with arsenic, **12**. Crystals

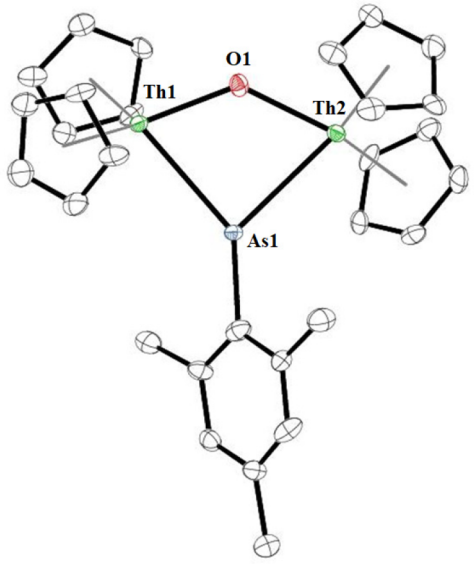


**Figure 8.** Thermal ellipsoid plot of **11**, shown at the 50% probability level. All hydrogens in the structure, and methyl groups on the $(C_5Me_5)^{-1}$ ligands, were omitted for clarity. Pertinent bond lengths and angles are as follows: Th1−As1, 2.8733(10) Å; Th2−As1, 2.8850(10); Th1−O1, 2.146(5) Å; Th2−O1, 2.151(5) Å; Th1−As1−Th2, 85.94(3)°; Th1−O1−Th2, 132.0(3)°.


https://doi.org/10.1021/acs.inorgchem.1c01256
Inorg. Chem. 2021, 60, 10614−10630

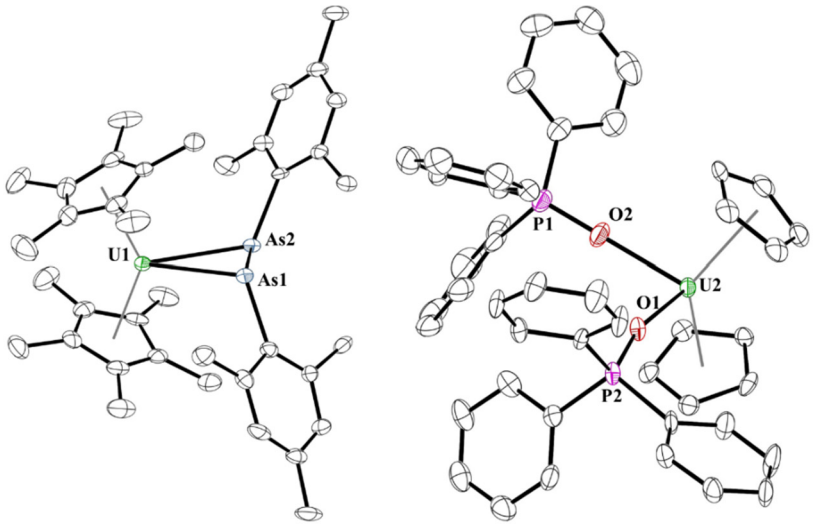


**Figure 9.** Thermal ellipsoid plot of **12** shown at the 50% probability level. All hydrogens and the methyl groups on the $(C_5Me_5)^{1-}$ ligands on the cationic complex were omitted for clarity. Pertinent bond distances and angles are as follows: U1−As1, 2.9814(8) Å; U1−As2, 2.9757(8) Å; As1−As2, 2.4671(8) Å; U2−O1, 2.361(4) Å; U2−O2, 2.359(3) Å.

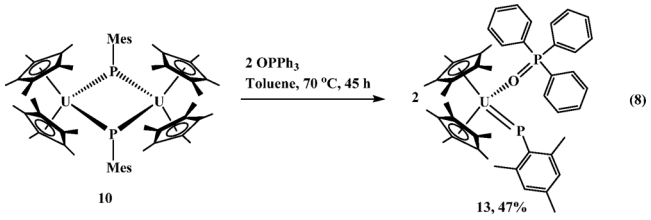


suitable for an X-ray crystallographic analysis were grown from a saturated diethyl ether solution at −40 °C, Figure 10.

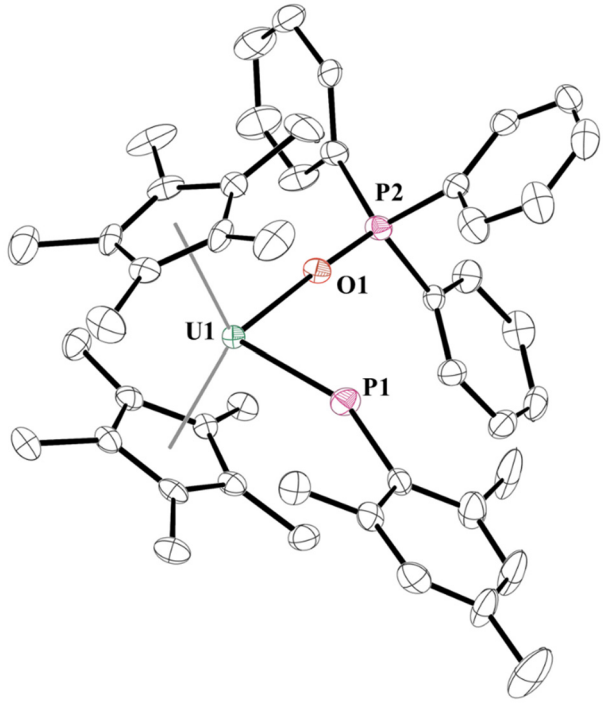


**Figure 10.** Thermal ellipsoid plot of **13** shown at the 50% probability level. The hydrogen atoms were omitted for clarity. Pertinent bond distances are angles are as follows: U1−P1, 2.5022(18) Å; U1−O1, 2.364(4) Å; U−P1−C(ipso): 156.8(2)°.

Complex **13** is nearly identical to the first uranium phosphinidene isolated, $(C_5Me_5)_2U(=PMes^*)(OPMe_3)$, Mes* = 2,4,6-$^t$Bu$_3$C$_6$H$_2$,[43] which has a U−P bond distance of 2.562(3) Å and U−P−C(*ipso*) angle of 143.7(3)°, while the U−P distance and U−P−C(*ipso*) angle in **9** are 2.502(2) Å and 156.8(2)°, respectively. In addition, these metrics can be compared to recent metallocene uranium phosphinidene complexes, $(1,2,4\text{-}^tBu_3C_5H_2)_2U{=}PMes^*$, with U−P length of 2.495(1) Å and U−P−C(*ipso*) angle of 177.4(1)°,[45] and $(1,3\text{-}^tBu_2C_5H_3)_2U(=PMes^*)(OPMe_3)$, with a U−P bond distance of 2.508(1) Å and U−P−C(*ipso*) angle of 162.8(1)°.[45]

Complex **13** was also analyzed by a QTAIM analysis. All complexes considered here show deviations larger than would be expected for a single bond; however, this is most pronounced in **13**, which might be expected to have a more developed multiple bond character. To further investigate potential multiple bond character, a natural bond order (NBO) analysis was performed. A qualitative analysis of the phosphinidene complexes revealed a single M-E $\sigma$-bond as well as two well-defined NBOs representing M-E $\pi$-bonding interactions, Figure 11. The delocalization index for **13** is 1.345, which can be compared to both the calculated thorium analogue of 1.19 as well as our previously reported thorium phosphinidene, $\{(C_5Me_5)_2Th(=PTipp)[P(H)Tipp]\}^{1-}$, which also has a DI of 1.19.[26]

Complex **13** shows a qualitatively different thermal magnetic susceptibility behavior compared to the other uranium complexes measured, in that it displays less temperature dependence at higher temperatures and shows a steeper downturn in the effective magnetic moment at lower temperatures, Figure 7. Of all the compounds studied here, **13** has the lowest symmetry ligand environment (one phosphinidene and one phosphine oxide). Interestingly, the initial slope of mononuclear P-containing **13** is comparable with the arsinidiide complex **8**.

## CONCLUSION

Overall, we have used a set of thorium and uranium complexes with phosphorus and arsenic bonds to examine differences in structure, bonding, and reactivity. In both cases, the bis(arsenido) complexes were thermally unstable and lose $H_2$ to


https://doi.org/10.1021/acs.inorgchem.1c01256
Inorg. Chem. 2021, 60, 10614−10630

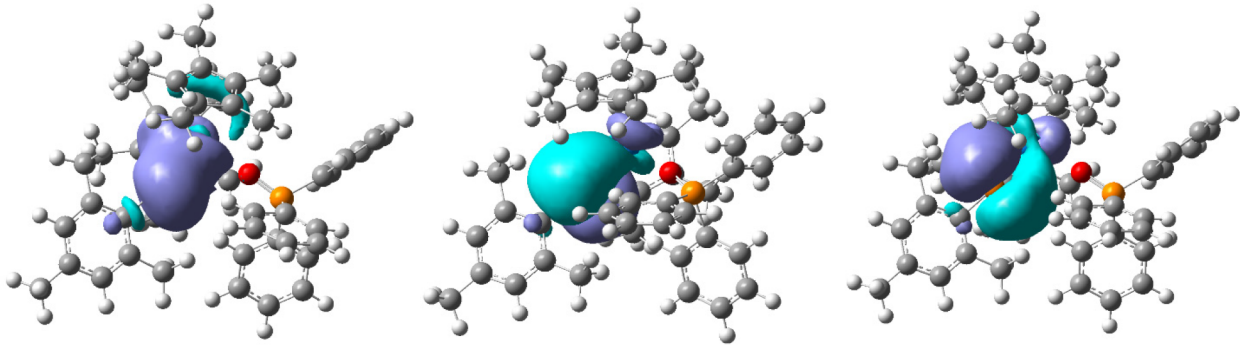

**Figure 11.** Uranium−Phosphorus $\sigma$-bond (left) and two $\pi$-bonds (middle and right), derived from NBO analyses.

form diarsenido moieties. In both cases, the arsinidiide complexes could be isolated, but only the uranium phosphinidiide could be synthesized. In the case of thorium, a C−H bond activation occurred, which is similar to calculations that were shown to form a thorium phosphinidiide previously. The reactivity of $OPPh_3$ was attempted to form terminal actinide-pnictinidene complexes; however, the uranium arsinidiide showed the ability for uranium−arsenic complexes to reduce to U(III), while an oxo transfer was observed with the thorium arsinidiide. In the case of the uranium phosphinidiide, a terminal phosphinidene could be isolated. Computational methods, in tandem with electrochemical and magnetic measurements, demonstrate that these bonds are highly polarized; thus, the electronegativity of phosphorus and arsenic drive their donating properties, which are nearly identical. The only difference in the crystal field was observed in the magnetic data that showed more excited-state mixing with the arsenic-containing uranium complexes versus those with phosphorus. A computational analysis also suggests that there is greater overlap-driven covalency in An-P bonds, and greater energy degeneracy-driven covalency in An-As bonds.[116] However, all of these complexes indicate that the energy-driven covalency concept does not have an effect on their stability or reactivity. It appears the electronegativity of phosphorus and arsenic, as well as the thermodynamics associated with E-E bond forming reactions with an incoming substrate, drive their chemistry. Now that we have established these starting materials, we anticipate their reactivity with small molecules will lead to exciting new results as we have observed previously with thorium and uranium−phosphorus bonds.[117,118]

## ■ ASSOCIATED CONTENT

### Supporting Information

The Supporting Information is available free of charge at https://pubs.acs.org/doi/10.1021/acs.inorgchem.1c01256.

NMR spectra, crystallographic, magnetic measurements, and computational details (PDF)

### Accession Codes

CCDC 1996293, 1996892, 1996917, 1998117, 1998572, 1998880, 2056207, 2056215, 2056283, 2056520−2056521, 2061431, and 2062035 contain the supplementary crystallographic data for this paper. These data can be obtained free of charge via www.ccdc.cam.ac.uk/data_request/cif, or by emailing data_request@ccdc.cam.ac.uk, or by contacting The Cambridge Crystallographic Data Centre, 12 Union Road, Cambridge CB2 1EZ, UK; fax: +44 1223 336033.

## ■ AUTHOR INFORMATION


### Corresponding Authors

**Justin R. Walensky** − *Department of Chemistry, University of Missouri, Columbia 65211, Missouri, United States;* orcid.org/0000-0003-0221-2675; Email: walenskyj@missouri.edu

**Matthew P. Shores** − *Department of Chemistry, Colorado State University, Fort Collins 80523, Colorado, United States;* orcid.org/0000-0002-9751-0490; Email: shores@colostate.edu

**Andrew Kerridge** − *Department of Chemistry, Lancaster University, Lancaster LA1 4YB, U.K.;* orcid.org/0000-0002-2876-1202; Email: a.kerridge@lancaster.ac.uk

### Authors

**Michael L. Tarlton** − *Department of Chemistry, University of Missouri, Columbia 65211, Missouri, United States*

**O. Jonathan Fajen** − *Department of Chemistry, University of Missouri, Columbia 65211, Missouri, United States*

**Steven P. Kelley** − *Department of Chemistry, University of Missouri, Columbia 65211, Missouri, United States;* orcid.org/0000-0001-6755-4495

**Thomas Malcomson** − *Department of Chemistry, Lancaster University, Lancaster LA1 4YB, U.K.*

**Thomas L. Morrison** − *Department of Chemistry, Colorado State University, Fort Collins 80523, Colorado, United States*

**Xhensila Xhani** − *Department of Chemistry, University of Missouri, Columbia 65211, Missouri, United States*

Complete contact information is available at: https://pubs.acs.org/10.1021/acs.inorgchem.1c01256


### Notes

The authors declare no competing financial interest.

## ■ ACKNOWLEDGMENTS

We gratefully acknowledge the Department of Energy, Office of Basic Energy Sciences, Heavy Element Program under Award No. DE-SC-0021273 (J.R.W.). T.M. and A.K. thank the High End Computing facility at Lancaster University. M.P.S. and T.L.M. thank the National Science Foundation (CHE-1956399) for support of the magnetometry measurements.

## ■ REFERENCES

(1) Xu, L.; Pu, N.; Li, Y.; Wei, P.; Sun, T.; Xiao, C.; Chen, J.; Xu, C. Selective Separation and Complexation of Trivalent Actinide and Lanthanide by a Tetradentate Soft−Hard Donor Ligand: Solvent Extraction, Spectroscopy, and DFT Calculations. *Inorg. Chem.* **2019**, *58*, 4420−4430.

(2) Lehman-Andino, I.; Su, J.; Papathanasiou, K. E.; Eaton, T. M.; Jian, J.; Dan, D.; Albrecht-Schmitt, T. E.; Dares, C. J.; Batista, E. R.; Yang, P.; Gibson, J. K.; Kavallieratos, K. Soft-donor dipicolinamide derivatives for selective actinide(iii)/lanthanide(iii) separation: the role of S- vs. O-donor sites. *Chem. Commun.* **2019**, *55*, 2441−2444.
(3) Grimes, T. S.; Heathman, C. R.; Jansone-Popova, S.; Ivanov, A. S.; Bryantsev, V. S.; Zalupski, P. R. Exploring Soft Donor Character of the N-2-Pyrazinylmethyl Group by Coordinating Trivalent Actinides and Lanthanides Using Aminopolycarboxylates. *Inorg. Chem.* **2020**, *59*, 138−150.
(4) Street, K.; Seaborg, G. T. The Separation of Americium and Curium from the Rare Earth Elements. *J. Am. Chem. Soc.* **1950**, *72*, 2790−2792.
(5) Diamond, R. M.; Street, K.; Seaborg, G. T. An Ion-exchange Study of Possible Hybridized 5f Bonding in the Actinides1. *J. Am. Chem. Soc.* **1954**, *76*, 1461−1469.
(6) Jensen, M. P.; Bond, A. H. Comparison of Covalency in the Complexes of Trivalent Actinide and Lanthanide Cations. *J. Am. Chem. Soc.* **2002**, *124*, 9870−9877.
(7) Bessen, N. P.; Jackson, J. A.; Jensen, M. P.; Shafer, J. C. Sulfur donating extractants for the separation of trivalent actinides and lanthanides. *Coord. Chem. Rev.* **2020**, *421*, 213446.
(8) Drader, J. A.; Luckey, M.; Braley, J. C. Thermodynamic Considerations of Covalency in Trivalent Actinide-(poly)-aminopolycarboxylate Interactions. *Solvent Extr. Ion Exch.* **2016**, *34*, 114−125.
(9) Kelley, M. P.; Su, J.; Urban, M.; Luckey, M.; Batista, E. R.; Yang, P.; Shafer, J. C. On the Origin of Covalent Bonding in Heavy Actinides. *J. Am. Chem. Soc.* **2017**, *139*, 9901−9908.
(10) Iversen, B. B.; Larsen, F. K.; Pinkerton, A. A.; Martin, A.; Darovsky, A.; Reynolds, P. A. Characterization of Actinide Bonding in $Th(S_2PMe_2)_4$ by Synchrotron X-ray Diffraction. *Inorg. Chem.* **1998**, *37*, 4559−4566.
(11) Gaunt, A. J.; Reilly, S. D.; Enriquez, A. E.; Scott, B. L.; Ibers, J. A.; Sekar, P.; Ingram, K. I. M.; Kaltsoyannis, N.; Neu, M. P. Experimental and Theoretical Comparison of Actinide and Lanthanide Bonding in $M[N(EPR_2)_2]_3$ Complexes (M = U, Pu, La, Ce; E = S, Se, Te; R = Ph, $^i$Pr, H). *Inorg. Chem.* **2008**, *47*, 29−41.
(12) Brown, J. L.; Fortier, S.; Lewis, R. A.; Wu, G.; Hayton, T. W. A Complete Family of Terminal Uranium Chalcogenides, $[U(E)(N\{SiMe_3\}_2)_3]^-$ (E = O, S, Se, Te). *J. Am. Chem. Soc.* **2012**, *134*, 15468−15475.
(13) Brown, J. L.; Fortier, S.; Wu, G.; Kaltsoyannis, N.; Hayton, T. W. Synthesis and Spectroscopic and Computational Characterization of the Chalcogenido-Substituted Analogues of the Uranyl Ion, $[OUE]_2^+$ (E = S, Se). *J. Am. Chem. Soc.* **2013**, *135*, 5352−5355.
(14) Behrle, A. C.; Kerridge, A.; Walensky, J. R. Dithio- and Diselenophosphinate Thorium(IV) and Uranium(IV) Complexes: Molecular and Electronic Structures, Spectroscopy, and Transmetalation Reactivity. *Inorg. Chem.* **2015**, *54*, 11625−11636.
(15) Matson, E. M.; Goshert, M. D.; Kiernicki, J. J.; Newell, B. S.; Fanwick, P. E.; Shores, M. P.; Walensky, J. R.; Bart, S. C. Synthesis of Terminal Uranium(IV) Disulfido and Diselenido Compounds by Activation of Elemental Sulfur and Selenium. *Chem. - Eur. J.* **2013**, *19*, 16176−16180.
(16) Jones, M. B.; Gaunt, A. J.; Gordon, J. C.; Kaltsoyannis, N.; Neu, M. P.; Scott, B. L. Uncovering f-element bonding differences and electronic structure in a series of 1:3 and 1:4 complexes with a diselenophosphinate ligand. *Chem. Sci.* **2013**, *4*, 1189−1203.
(17) Matson, E. M.; Breshears, A. T.; Kiernicki, J. J.; Newell, B. S.; Fanwick, P. E.; Shores, M. P.; Walensky, J. R.; Bart, S. C. Trivalent Uranium Phenylchalcogenide Complexes: Exploring the Bonding and Reactivity with $CS_2$ in the $Tp^*_2UEPh$ Series (E = O, S, Se, Te). *Inorg. Chem.* **2014**, *53* (24), 12977−12985.
(18) Smiles, D. E.; Wu, G.; Hrobárik, P.; Hayton, T. W. Use of $^{77}$Se and $^{125}$Te NMR Spectroscopy to Probe Covalency of the Actinide-Chalcogen Bonding in $[Th(En)\{N(SiMe_3)_2\}_3]^-$ (E = Se, Te; n = 1, 2) and Their Oxo-Uranium(VI) Congeners. *J. Am. Chem. Soc.* **2016**, *138*, 814−825.
(19) Wu, W.; Rehe, D.; Hrobárik, P.; Kornienko, A. Y.; Emge, T. J.; Brennan, J. G. Molecular Thorium Compounds with Dichalcogenide Ligands: Synthesis, Structure, $^{77}$Se NMR Study, and Thermolysis. *Inorg. Chem.* **2018**, *57*, 14821−14833.
(20) Ringgold, M.; Rehe, D.; Hrobárik, P.; Kornienko, A. Y.; Emge, T. J.; Brennan, J. G. Thorium Cubanes−Synthesis, Solid-State and Solution Structures, Thermolysis, and Chalcogen Exchange Reactions. *Inorg. Chem.* **2018**, *57*, 7129−7141.
(21) Rookes, T. M.; Wildman, E. P.; Balázs, G.; Gardner, B. M.; Wooles, A. J.; Gregson, M.; Tuna, F.; Scheer, M.; Liddle, S. T. Actinide−Pnictide (An−Pn) Bonds Spanning Non-Metal, Metalloid, and Metal Combinations (An = U, Th; Pn = P, As, Sb, Bi). *Angew. Chem., Int. Ed.* **2018**, *57*, 1332−1336.
(22) Behrle, A. C.; Barnes, C. L.; Kaltsoyannis, N.; Walensky, J. R. Systematic Investigation of Thorium(IV)− and Uranium(IV)−Ligand Bonding in Dithiophosphonate, Thioselenophosphinate, and Diselenophosphonate Complexes. *Inorg. Chem.* **2013**, *52*, 10623−10631.
(23) Gardner, B. M.; Balázs, G.; Scheer, M.; Tuna, F.; McInnes, E. J. L.; McMaster, J.; Lewis, W.; Blake, A. J.; Liddle, S. T. Triamidoamine uranium(IV)−arsenic complexes containing one-, two- and threefold U−As bonding interactions. *Nat. Chem.* **2015**, *7*, 582.
(24) Gardner, B. M.; Balázs, G.; Scheer, M.; Wooles, A. J.; Tuna, F.; McInnes, E. J. L.; McMaster, J.; Lewis, W.; Blake, A. J.; Liddle, S. T. Isolation of Elusive HAsAsH in a Crystalline Diuranium(IV) Complex. *Angew. Chem., Int. Ed.* **2015**, *54*, 15250−15254.
(25) Behrle, A. C.; Walensky, J. R. Insertion of $^t$BuNC into thorium−phosphorus and thorium−arsenic bonds: phosphaazaallene and arsaazaallene moieties in f element chemistry. *Dalton Trans.* **2016**, *45*, 10042−10049.
(26) Vilanova, S. P.; Alayoglu, P.; Heidarian, M.; Huang, P.; Walensky, J. R. Metal−Ligand Multiple Bonding in Thorium Phosphorus and Thorium Arsenic Complexes. *Chem. - Eur. J.* **2017**, *23*, 16748−16752.
(27) Wildman, E. P.; Balázs, G.; Wooles, A. J.; Scheer, M.; Liddle, S. T. Triamidoamine thorium-arsenic complexes with parent arsenide, arsinidiide and arsenido structural motifs. *Nat. Commun.* **2017**, *8*, 14769.
(28) Hoerger, C. J.; Heinemann, F. W.; Louyriac, E.; Rigo, M.; Maron, L.; Grützmacher, H.; Driess, M.; Meyer, K. Cyaarside ($CAs^-$) and 1,3-Diarsaallendiide ($AsCAs_2^-$) Ligands Coordinated to Uranium and Generated via Activation of the Arsaethynolate Ligand ($OCAs^-$). *Angew. Chem., Int. Ed.* **2019**, *58*, 1679−1683.
(29) Andrews, L.; Wang, X.; Roos, B. O. As≡$UF_3$ Molecule with a Weak Triple Bond to Uranium. *Inorg. Chem.* **2009**, *48*, 6594−6598.
(30) Rozenel, S. S.; Edwards, P. G.; Petrie, M. A.; Andersen, R. A. Eight coordinate 1,2-bis(dimethylarsino) and 1,2-bis-(dimethylphosphino)-benzene complexes of uranium tetrachloride, $UCl_4[(1,2\text{-}Me_2E)_2C_6H_4]_2$ where E is As or P. *Polyhedron* **2016**, *116*, 122−126.
(31) Scherer, O. J.; Schulze, J.; Wolmershäuser, G. Bicyclisches $As_6$ als komplexligand. *J. Organomet. Chem.* **1994**, *484*, c5−c7.
(32) Walensky, J. R.; Martin, R. L.; Ziller, J. W.; Evans, W. J. Importance of Energy Level Matching for Bonding in $Th^{3+}$-$Am^{3+}$ Actinide Metallocene Amidinates, $(C_5Me_5)_2[^iPrNC(Me)N^iPr]An$. *Inorg. Chem.* **2010**, *49*, 10007−10012.
(33) Su, J.; Batista, E. R.; Boland, K. S.; Bone, S. E.; Bradley, J. A.; Cary, S. K.; Clark, D. L.; Conradson, S. D.; Ditter, A. S.; Kaltsoyannis, N.; Keith, J. M.; Kerridge, A.; Kozimor, S. A.; Löble, M. W.; Martin, R. L.; Minasian, S. G.; Mocko, V.; La Pierre, H. S.; Seidler, G. T.; Shuh, D. K.; Wilkerson, M. P.; Wolfsberg, L. E.; Yang, P. Energy-Degeneracy-Driven Covalency in Actinide Bonding. *J. Am. Chem. Soc.* **2018**, *140*, 17977−17984.
(34) Platts, J. A.; Baker, R. J. A computational investigation of orbital overlap versus energy degeneracy covalency in $[UE_2]_2^+$ (E = O, S, Se, Te) complexes. *Dalton Transs* **2020**, *49*, 1077−1088.
(35) Huang, Q.-R.; Kingham, J. R.; Kaltsoyannis, N. The strength of actinide−element bonds from the quantum theory of atoms-in-molecules. *Dalton Trans.* **2015**, *44*, 2554−2566.


https://doi.org/10.1021/acs.inorgchem.1c01256
*Inorg. Chem.* 2021, 60, 10614−10630

(36) Actinides: Pnictogen Complexes. In *Encyclopedia of Inorganic and Bioinorganic Chemistry*; Wiley, pp 1−17. DOI: 10.1002/9781119951438
(37) Zhang, C.; Hou, G.; Zi, G.; Walter, M. D. A base-free terminal thorium phosphinidene metallocene and its reactivity toward selected organic molecules. *Dalton Trans.* **2019**, *48*, 2377−2387.
(38) Scherer, O. J.; Werner, B.; Heckmann, G.; Wolmershäuser, G. Bicyclic $P_6$ as Complex Ligand. *Angew. Chem., Int. Ed. Engl.* **1991**, *30*, 553−555.
(39) Zhang, C.; Wang, Y.; Hou, G.; Ding, W.; Zi, G.; Walter, M. D. Experimental and computational studies on a three-membered diphosphido thorium metallaheterocycle $[\eta^5$-1,3-$(Me_3C)_2C_5H_3]_2$Th-$[\eta^2$-$P_2(2,4,6$-$^iPr_3C_6H_2)_2]$. *Dalton Trans.* **2019**, *48*, 6921−6930.
(40) Behrle, A. C.; Castro, L.; Maron, L.; Walensky, J. R. Formation of a Bridging Phosphinidene Thorium Complex. *J. Am. Chem. Soc.* **2015**, *137*, 14846−14849.
(41) Zhang, C.; Hou, G.; Zi, G.; Ding, W.; Walter, M. D. An Alkali-Metal Halide-Bridged Actinide Phosphinidiide Complex. *Inorg. Chem.* **2019**, *58*, 1571−1590.
(42) Wang, Y.; Zhang, C.; Zi, G.; Ding, W.; Walter, M. D. Preparation of a potassium chloride bridged thorium phosphinidiide complex and its reactivity towards small organic molecules. *New J. Chem.* **2019**, *43*, 9527−9539.
(43) Arney, D. S. J.; Schnabel, R. C.; Scott, B. C.; Burns, C. J. Preparation of Actinide Phosphinidene Complexes: Steric Control of Reactivity. *J. Am. Chem. Soc.* **1996**, *118*, 6780−6781.
(44) Zhang, C.; Hou, G.; Zi, G.; Ding, W.; Walter, M. D. A Base-Free Terminal Actinide Phosphinidene Metallocene: Synthesis, Structure, Reactivity, and Computational Studies. *J. Am. Chem. Soc.* **2018**, *140*, 14511−14525.
(45) Wang, D.; Wang, S.; Hou, G.; Zi, G.; Walter, M. D. A Lewis Base Supported Terminal Uranium Phosphinidene Metallocene. *Inorg. Chem.* **2020**, *59*, 14549−14563.
(46) Wang, D.; Hou, G.; Zi, G.; Walter, M. D. $(\eta^5$-$C_5Me_5)_2$U(=P-2,4,6-$^tBu_3C_6H_2)(OPMe_3)$ Revisited—Its Intrinsic Reactivity toward Small Organic Molecules. *Organometallics* **2020**, *39*, 4085−4101.
(47) Wang, D.; Hou, G.; Zi, G.; Walter, M. D. Influence of the Lewis Base Ph3PO on the Reactivity of the Uranium Phosphinidene $(\eta^5$-$C_5Me_5)_2$U(=P-2,4,6-$^iPr_3C_6H_2)(OPPh_3)$. *Organometallics* **2021**, *40*, 383−396.
(48) Wang, D.; Ding, W.; Hou, G.; Zi, G.; Walter, M. D. Experimental and Computational Studies on a Base-Free Terminal Uranium Phosphinidene Metallocene. *Chem. - Eur. J.* **2020**, *26*, 16888−16899.
(49) Wang, X.; Andrews, L. Infrared spectra and density functional calculations of triplet pnictinidene N÷ThF3, P÷$ThF_3$ and As÷$ThF_3$ molecules. *Dalton Trans.* **2009**, 9260−9265.
(50) Andrews, L.; Cho, H.-G.; Thanthiriwatte, K. S.; Dixon, D. A. Thorium and Uranium Hydride Phosphorus and Arsenic Bearing Molecules with Single and Double Actinide-Pnictogen and Bridged Agostic Hydrogen Bonds. *Inorg. Chem.* **2017**, *56*, 2949−2957.
(51) Du, J.; Hunger, D.; Seed, J. A.; Cryer, J. D.; King, D. M.; Wooles, A. J.; van Slageren, J.; Liddle, S. T. Dipnictogen f-Element Chemistry: A Diphosphorus Uranium Complex. *J. Am. Chem. Soc.* **2021**, *143*, 5343−5348.
(52) Pugh, T.; Kerridge, A.; Layfield, R. A. Yttrium Complexes of Arsine, Arsenide, and Arsinidene Ligands. *Angew. Chem., Int. Ed.* **2015**, *54*, 4255−4258.
(53) Kurz, S.; Oesen, H.; Sieler, J.; Hey-hawkins, E. SYNTHESIS AND MOLECULAR STRUCTURE OF Mes(H)P-P(H)Mes (Mes = 2,4,6-$Me_3C_6H_2$). *Phosphorus, Sulfur Silicon Relat. Elem.* **1996**, *117*, 189−196.
(54) Pagano, J. K.; Dorhout, J. M.; Waterman, R.; Czerwinski, K. R.; Kiplinger, J. L. Phenylsilane as a safe, versatile alternative to hydrogen for the synthesis of actinide hydrides. *Chem. Commun.* **2015**, *51*, 17379−17381.
(55) Rungthanaphatsophon, P.; Bathelier, A.; Castro, L.; Behrle, A. C.; Barnes, C. L.; Maron, L.; Walensky, J. R. Formation of Methane versus Benzene in the Reactions of $(C_5Me_5)_2Th(CH_3)_2$ with $[CH_3PPh_3]_X$ (X = Cl, Br, I) Yielding Thorium-Carbene or Thorium-Ylide Complexes. *Angew. Chem., Int. Ed.* **2017**, *56*, 12925−12929.
(56) Bain, G. A.; Berry, J. F. Diamagnetic Corrections and Pascal's Constants. *J. Chem. Educ.* **2008**, *85*, 532.
(57) Adamo, C.; Barone, V. Toward reliable density functional methods without adjustable parameters: The PBE0 model. *J. Chem. Phys.* **1999**, *110*, 6158−6170.
(58) Ernzerhof, M.; Scuseria, G. E. Assessment of the Perdew−Burke−Ernzerhof exchange-correlation functional. *J. Chem. Phys.* **1999**, *110*, 5029−5036.
(59) Weigend, F.; Ahlrichs, R. Balanced basis sets of split valence, triple zeta valence and quadruple zeta valence quality for H to Rn: Design and assessment of accuracy. *Phys. Chem. Chem. Phys.* **2005**, *7*, 3297−3305.
(60) Cao, X.; Dolg, M.; Stoll, H. Valence basis sets for relativistic energy-consistent small-core actinide pseudopotentials. *J. Chem. Phys.* **2003**, *118*, 487−496.
(61) Cao, X.; Dolg, M. Segmented contraction scheme for small-core actinide pseudopotential basis sets. *J. Mol. Struct.: THEOCHEM* **2004**, *673*, 203−209.
(62) Küchle, W.; Dolg, M.; Stoll, H.; Preuss, H. Energy-adjusted pseudopotentials for the actinides. Parameter sets and test calculations for thorium and thorium monoxide. *J. Chem. Phys.* **1994**, *100*, 7535−7542.
(63) Balasubramani, S. G.; Chen, G. P.; Coriani, S.; Diedenhofen, M.; Frank, M. S.; Franzke, Y. J.; Furche, F.; Grotjahn, R.; Harding, M. E.; Hattig, C.; Hellweg, A.; Helmich-Paris, B.; Holzer, C.; Huniar, U.; Kaupp, M.; Marefat Khah, A.; Karbalaei Khani, S.; Muller, T.; Mack, F.; Nguyen, B. D.; Parker, S. M.; Perlt, E.; Rappoport, D.; Reiter, K.; Roy, S.; Ruckert, M.; Schmitz, G.; Sierka, M.; Tapavicza, E.; Tew, D. P.; van Wullen, C.; Voora, V. K.; Weigend, F.; Wodynski, A.; Yu, J. M. TURBOMOLE: Modular program suite for ab initio quantum-chemical and condensed-matter simulations. *J. Chem. Phys.* **2020**, *152*, 184107.
(64) Glendening, E. D.; Badenhoop, J. K., Reed, A. E.; Carpenter, J. E.; Bohmann, J. A.; Morales, C. M.; Landis, C. R.; Weinhold, F. *NBP Homepage*; Theoretical Chemistry Institute, University of Wisconsin, Madison, WI, 2013); http://nbo6.chem.wisc.edu/.
(65) Dennington, R.; Keith, T. A.; Millam, J. M. *GaussView,* ver. 5.0; Semichem Inc.: Shawnee Mission, KS, 2009.
(66) Keith, T. A. *AIMAll;* Gristmill Software: Overland Park, KS, 2019.
(67) Tarlton, M. L.; Del Rosal, I.; Vilanova, S. P.; Kelley, S. P.; Maron, L.; Walensky, J. R. Comparative Insertion Reactivity of CO, $CO_2$, $^t$BuCN, and $^t$BuNC into Thorium− and Uranium−Phosphorus Bonds. *Organometallics* **2020**, *39*, 2152−2161.
(68) Magnall, R.; Balazs, G.; Lu, E.; Kern, M.; Slageren, J.; Tuna, F.; Wooles, A. J.; Scheer, M.; Liddle, S. T. Photolytic and Reductive Activations of 2-Arsaethynolate in a Uranium−Triamidoamine Complex: Decarbonylative Arsenic-Group Transfer Reactions and Trapping of a Highly Bent and Reduced Form. *Chem. - Eur. J.* **2019**, *25*, 14246−14252.
(69) Bugaris, D. E.; Ibers, J. A. Syntheses and characterization of some solid-state actinide (Th, U, Np) compounds. *Dalton Trans.* **2010**, *39*, 5949−5964.
(70) Elmes, P. S.; Leverett, P.; West, B. O. X-Ray determination of the structure of Fe(CO)4(AsC6F5)2, a complex containing "decafluoro-arsenobenzene. *J. Chem. Soc. D* **1971**, *0*, 747b−748.
(71) Schmidt, M.; Konieczny, D.; Peresypkina, E. V.; Virovets, A. V.; Balázs, G.; Bodensteiner, M.; Riedlberger, F.; Krauss, H.; Scheer, M. Arsenic-Rich Polyarsenides Stabilized by Cp*Fe Fragments. *Angew. Chem., Int. Ed.* **2017**, *56*, 7307−7311.
(72) Spitzer, F.; Sierka, M.; Latronico, M.; Mastrorilli, P.; Virovets, A. V.; Scheer, M. Fixation and Release of Intact $E_4$ Tetrahedra (E = P, As). *Angew. Chem., Int. Ed.* **2015**, *54* (14), 4392−4396.
(73) Arleth, N.; Gamer, M. T.; Köppe, R.; Konchenko, S. N.; Fleischmann, M.; Scheer, M.; Roesky, P. W. Molecular Polyarsenides of the Rare-Earth Elements. *Angew. Chem., Int. Ed.* **2016**, *55*, 1557−1560.

(74) Dütsch, L.; Fleischmann, M.; Welsch, S.; Balázs, G.; Kremer, W.; Scheer, M. Dicationic $E_4$ Chains (E = P, As, Sb, Bi) Embedded in the Coordination Sphere of Transition Metals. *Angew. Chem., Int. Ed.* **2018**, *57*, 3256−3261.
(75) Hierlmeier, G.; Hinz, A.; Wolf, R.; Goicoechea, J. M. Synthesis and Reactivity of Nickel-Stabilised $\mu^2$:$\eta^2$,$\eta^2$-$P_2$, $As_2$ and PAs Units. *Angew. Chem., Int. Ed.* **2018**, *57*, 431−436.
(76) Blacque, O.; Brunner, H.; M Kubicki, M.; Leis, F.; Lucas, D.; Mugnier, Y.; Nuber, B.; Wachter, J. Structural Rearrangements in Triple-Decker-Like Complexes with Mixed Group 15/16 Ligands: Synthesis and Characterization of the Redox Couple $[Cp_2{*}Fe_2As_2Se_2]$/$[Cp_2{*}Fe_2As_2Se_2]^+$ (Cp*=$C_5Me_5$). *Chem. - Eur. J.* **2001**, *7*, 1342−1349.
(77) McGrath, M.; Spalding, T. R.; Fontaine, X. L. R.; Kennedy, J. D.; Thornton-Pett, M. Metallaheteroborane chemistry. Part 9. Syntheses and spectroscopy of platinum and palladium phosphine complexes containing $\eta^5$-{$As_2B_9$}-based cluster ligands. Crystal structures of [3,3-L2-closo-3,1,2-$PtAs_2B_9H_9$](L = $PPh_3$ or $PMe_2Ph$) and [3-Cl-3,8-$(PPh_3)_2$-closo-3,1,2-$PdAs_2B_9H_8$]. *J. Chem. Soc., Dalton Trans.* **1991**, 3223−3233.
(78) McLellan, R.; Boag, N. M.; Dodds, K.; Ellis, D.; Macgregor, S. A.; McKay, D.; Masters, S. L.; Noble-Eddy, R.; Platt, N. P.; Rankin, D. W. H.; Robertson, H. E.; Rosair, G. M.; Welch, A. J. New chemistry of 1,2-closo-$P_2B_{10}H_{10}$ and 1,2-closo-$As_2B_{10}H_{10}$; in silico and gas electron diffraction structures, and new metalladiphospha- and metalladiarsaboranes. *Dalton Trans.* **2011**, *40*, 7181−7192.
(79) Ferguson, G.; Gallagher, J. F.; Kennedy, J. D.; Kelleher, A.-M.; Spalding, T. R. Pentahapto-bonded gold heteroborane clusters [3-$(R_3P)$-closo-2,1-$AuTeB_{10}H_{10}$]$^-$ and [3-$(R_3P)$-closo-3,1,2-$AuAs_2B_9H_9$]$^-$. *Dalton Trans.* **2006**, 2133−2139.
(80) O'Connell, D.; Patterson, J. C.; Spalding, T. R.; Ferguson, G.; Gallagher, J. F.; Li, Y.; Kennedy, J. D.; Macías, R.; Thornton-Pett, M.; Holub, J. Conformational polymorphism and fluxional behaviour of $M(PR_3)_2$ units in closo-twelve-atom metallaheteroboranes with $MX_2B_9$(X = C or As) and MZB10 cages (Z = S, Se or Te). *J. Chem. Soc., Dalton Trans.* **1996**, 3323−3333.
(81) Jasper, S. A.; Roach, S.; Stipp, J. N.; Huffman, J. C.; Todd, L. J. The synthesis and chemistry of icosahedral bis(phosphine)-metalladiarsaboranes and -distibaboranes containing nickel and palladium. Crystal and molecular structures of closo-1,1-(Me2PPh)-2−1,2,3-PdAs2$B_9H_9$, closo-1,6-$Cl_2$-1,5-$(Me_2PPh)_2$-1,2,3-$PdAs_2B_9H_7.CH_2Cl_2$, and closo-1,1-$(Me_2PPh)_2$-1,2,3-$PdSb_2B_9H_9$. *Inorg. Chem.* **1993**, *32*, 3072−3080.
(82) Ferguson, G.; Li, Y.; Spalding, T. R.; Patterson, J. C. 3-tert-Butyl isocyanide)-3,8-bis(dimethylphenylphosphine)octahydro-1,2-diarsa-3-pallada-closo-dodecaboron(1+) Hexafluoroantimonate. *Acta Crystallogr., Sect. C: Cryst. Struct. Commun.* **1995**, *51*, 1498−1500.
(83) Chen, H.; Olmstead, M. M.; Pestana, D. C.; Power, P. P. Reactions of low-coordinate transition-metal amides with secondary phosphanes and arsanes: synthesis, structural, and spectroscopic studies of $[M\{N(SiMe_3)_2\}(\mu\text{-}PMes_2)]_2$ (M = manganese, iron), $[Mn\{N(SiMe_3)_2\}(\mu\text{-}AsMes_2)]_2$ and $Mes_2AsAsMes_2$. *Inorg. Chem.* **1991**, *30*, 1783−1787.
(84) Schumann, A.; Bresien, J.; Fischer, M.; Hering-Junghans, C. Aryl-substituted triarsiranes: synthesis and reactivity. *Chem. Commun.* **2021**, *57*, 1014−1017.
(85) Brookhart, M.; Green, M. L. H.; Parkin, G. Agostic interactions in transition metal compounds. *Proc. Natl. Acad. Sci. U. S. A.* **2007**, *104*, 6908−6914.
(86) Kiplinger, J. L.; Scott, B. L.; Schelter, E. J.; Pool Davis Tournear, J. A. Pool Davis Tournear, J. A. $sp^3$ versus $sp^2$ C−H bond activation chemistry of 2-picoline by Th(IV) and U(IV) metallocene complexes. *J. Alloys Compd.* **2007**, *444−445*, 477−482.
(87) Watt, F. A.; McCabe, K. N.; Schoch, R.; Maron, L.; Hohloch, S. A transient lanthanum phosphinidene complex. *Chem. Commun.* **2020**, *56*, 15410−15413.
(88) Vilanova, S. P.; Tarlton, M. L.; Barnes, C. L.; Walensky, J. R. Double insertion of benzophenone into thorium-phosphorus bonds. *J. Organomet. Chem.* **2018**, *857*, 159−163.
(89) Hou, Z.; Breen, T. L.; Stephan, D. W. Formation and reactivity of the early metal phosphides and phosphinidenes $Cp^*_2Zr$:PR, $Cp^*_2Zr(PR)_2$, and $Cp^*_2Zr(PR)_3$. *Organometallics* **1993**, *12*, 3158−3167.
(90) Benac, B. L.; Jones, R. A. Triphosphanato ($R_3P_3^{2-}$), primary phosphido ($RPH^-$) and diphosphanato (diphosphene) ($R_2P_2^{2-}$) complexes of zirconium and hafnium metallocenes. *Polyhedron* **1989**, *8*, 1774−1777.
(91) Kozimor, S. A.; Yang, P.; Batista, E. R.; Boland, K. S.; Burns, C. J.; Clark, D. L.; Conradson, S. D.; Martin, R. L.; Wilkerson, M. P.; Wolfsberg, L. E. Trends in Covalency for d- and f-Element Metallocene Dichlorides Identified Using Chlorine K-Edge X-ray Absorption Spectroscopy and Time-Dependent Density Functional Theory. *J. Am. Chem. Soc.* **2009**, *131*, 12125−12136.
(92) Schumann, A.; Reiß, F.; Jiao, H.; Rabeah, J.; Siewert, J.-E.; Krummenacher, I.; Braunschweig, H.; Hering-Junghans, C. A selective route to aryl-triphosphiranes and their titanocene-induced fragmentation. *Chem. Sci.* **2019**, *10*, 7859−7867.
(93) Gardner, B. M.; Balázs, G.; Scheer, M.; Tuna, F.; McInnes, E. J. L.; McMaster, J.; Lewis, W.; Blake, A. J.; Liddle, S. T. Triamidoamine−Uranium(IV)-Stabilized Terminal Parent Phosphide and Phosphinidene Complexes. *Angew. Chem., Int. Ed.* **2014**, *53*, 4484−4488.
(94) Leszczynski, J.; Kwiatkowski, J. S.; Leszczynska, D. Is the structure of selenoformamide similar to those of formamide and thioformamide? *J. Am. Chem. Soc.* **1992**, *114*, 10089−10091.
(95) Hall, S. W.; Huffman, J. C.; Miller, M. M.; Avens, L. R.; Burns, C. J.; Sattelberger, A. P.; Arney, D. S. J.; England, A. F. Synthesis and characterization of bis(pentamethylcyclopentadienyl)uranium(IV) and -thorium(IV) compounds containing the bis(trimethylsilyl)phosphide ligand. *Organometallics* **1993**, *12*, 752−758.
(96) Rungthanaphatsophon, P.; Duignan, T. J.; Myers, A. J.; Vilanova, S. P.; Barnes, C. L.; Autschbach, J.; Batista, E. R.; Yang, P.; Walensky, J. R. Influence of Substituents on the Electronic Structure of Mono- and Bis(phosphido) Thorium(IV) Complexes. *Inorg. Chem.* **2018**, *57*, 7270−7278.
(97) Rungthanaphatsophon, P.; Rosal, I. d.; Ward, R. J.; Vilanova, S. P.; Kelley, S. P.; Maron, L.; Walensky, J. R. Formation of an $\alpha$-Diimine from Isocyanide Coupling Using Thorium(IV) and Uranium(IV) Phosphido−Methyl Complexes. *Organometallics* **2019**, *38*, 1733−1740.
(98) Duttera, M. R.; Day, V. W.; Marks, T. J. Organoactinide phosphine/phosphite coordination chemistry. Facile hydride-induced dealkoxylation and the formation of actinide phosphinidene complexes. *J. Am. Chem. Soc.* **1984**, *106*, 2907−2912.
(99) Wildman, E. P.; Balázs, G.; Wooles, A. J.; Scheer, M.; Liddle, S. T. Thorium−phosphorus triamidoamine complexes containing Th−P single- and multiple-bond interactions. *Nat. Commun.* **2016**, *7*, 12884.
(100) Elkechai, A.; Mani, Y.; Boucekkine, A.; Ephritikhine, M. Density Functional Theory Investigation of the Redox Properties of Tricyclopentadienyl- and Phospholyluranium(IV) Chloride Complexes. *Inorg. Chem.* **2012**, *51*, 6943−6952.
(101) Kahan, R. J.; Cloke, F. G. N.; Roe, S. M.; Nief, F. Activation of carbon dioxide by new mixed sandwich uranium(iii) complexes incorporating cyclooctatetraenyl and pyrrolide, phospholide, or arsolide ligands. *New J. Chem.* **2015**, *39*, 7602−7607.
(102) Morris, D. E.; Da Re, R. E.; Jantunen, K. C.; Castro-Rodriguez, I.; Kiplinger, J. L. Trends in Electronic Structure and Redox Energetics for Early-Actinide Pentamethylcyclopentadienyl Complexes. *Organometallics* **2004**, *23*, 5142−5153.
(103) Graves, C. R.; Scott, B. L.; Morris, D. E.; Kiplinger, J. L. Facile Access to Pentavalent Uranium Organometallics: One-Electron Oxidation of Uranium(IV) Imido Complexes with Copper(I) Salts. *J. Am. Chem. Soc.* **2007**, *129*, 11914−11915.
(104) Pauling, L. *The Nature of The Chemical Bond;* Cornell University Press, 1961.
(105) Rookes, T. M.; Gardner, B. M.; Balázs, G.; Gregson, M.; Tuna, F.; Wooles, A. J.; Scheer, M.; Liddle, S. T. Crystalline Diuranium Phosphinidiide and $\mu$-Phosphido Complexes with Symmetric and Asymmetric UPU Cores. *Angew. Chem., Int. Ed.* **2017**, *56*, 10495−10500.


https://doi.org/10.1021/acs.inorgchem.1c01256
*Inorg. Chem.* 2021, 60, 10614−10630

(106) Schelter, E. J.; Yang, P.; Scott, B. L.; Thompson, J. D.; Martin, R. L.; Hay, P. J.; Morris, D. E.; Kiplinger, J. L. Systematic Studies of Early Actinide Complexes: Uranium(IV) Fluoroketimides. *Inorg. Chem.* **2007**, *46*, 7477−7488.
(107) Gardner, B. M.; King, D. M.; Tuna, F.; Wooles, A. J.; Chilton, N. F.; Liddle, S. T. Assessing crystal field and magnetic interactions in diuranium-$\mu$-chalcogenide triamidoamine complexes with UIV−E−UIV cores (E = S, Se, Te): implications for determining the presence or absence of actinide−actinide magnetic exchange. *Chem. Sci.* **2017**, *8*, 6207−6217.
(108) Tatebe, C. J.; Tong, Z.; Kiernicki, J. J.; Coughlin, E. J.; Zeller, M.; Bart, S. C. Activation of Triphenylphosphine Oxide Mediated by Trivalent Organouranium Species. *Organometallics* **2018**, *37*, 934−940.
(109) Evans, W. J.; Grate, J. W.; Bloom, I.; Hunter, W. E.; Atwood, J. L. Synthesis and x-ray crystallographic characterization of an oxo-bridged bimetallic organosamarium complex, $[(C_5Me_5)_2Sm]_2(\mu\text{-O})$. *J. Am. Chem. Soc.* **1985**, *107*, 405−409.
(110) Brennan, J. G.; Andersen, R. A.; Zalkin, A. Chemistry of trivalent uranium metallocenes: electron-transfer reactions. Synthesis and characterization of $[(MeC_5H_4)_3U]_2E$ (E = S, Se, Te) and the crystal structures of hexakis(methylcyclopentadienyl)sulfidodiuranium and tris(methylcyclopentadienyl)(triphenylphosphine oxide)uranium. *Inorg. Chem.* **1986**, *25*, 1761−1765.
(111) Podyacheva, E.; Kuchuk, E.; Chusov, D. Reduction of phosphine oxides to phosphines. *Tetrahedron Lett.* **2019**, *60*, 575−582.
(112) Manabe, S.; Wong, C. M.; Sevov, C. S. Direct and Scalable Electroreduction of Triphenylphosphine Oxide to Triphenylphosphine. *J. Am. Chem. Soc.* **2020**, *142*, 3024−3031.
(113) Chakraborty, B.; Menezes, P. W.; Driess, M. Beyond $CO_2$ Reduction: Vistas on Electrochemical Reduction of Heavy Non-metal Oxides with Very Strong E—O Bonds (E = Si, P, S). *J. Am. Chem. Soc.* **2020**, *142*, 14772−14788.
(114) Elias, J. S.; Costentin, C.; Nocera, D. G. Direct Electrochemical P(V) to P(III) Reduction of Phosphine Oxide Facilitated by Triaryl Borates. *J. Am. Chem. Soc.* **2018**, *140*, 13711−13718.
(115) Ren, W.; Zi, G.; Fang, D.-C.; Walter, M. D. Thorium Oxo and Sulfido Metallocenes: Synthesis, Structure, Reactivity, and Computational Studies. *J. Am. Chem. Soc.* **2011**, *133*, 13183−13196.
(116) Cooper, S.; Kaltsoyannis, N. Covalency in $AnCl_3$ (An = Th−No). *Dalton Trans.* **2021**, *50*, 1478−1485.
(117) Ward, R. J.; Rungthanaphatsophon, P.; Rosal, I. d.; Kelley, S. P.; Maron, L.; Walensky, J. R. Divergent uranium- versus phosphorus-based reduction of $Me_3SiN_3$ with steric modification of phosphido ligands. *Chem. Sci.* **2020**, *11*, 5830−5835.
(118) Vilanova, S. P.; del Rosal, I.; Tarlton, M. L.; Maron, L.; Walensky, J. R. Functionalization of Carbon Monoxide and *tert*-Butyl Nitrile by Intramolecular Proton Transfer in a Bis(Phosphido) Thorium Complex. *Angew. Chem., Int. Ed.* **2018**, *57*, 16748−16753.


https://doi.org/10.1021/acs.inorgchem.1c01256
*Inorg. Chem.* 2021, 60, 10614−10630